Electronic Research Archive

https://www.aimspress.com/journal/era

ERA, 34(5): 2974–3007.
DOI: 10.3934/era.2026135
Received: 27 December 2025
Revised: 28 February 2026
Accepted: 25 March 2026
Published: 07 April 2026

Research article

A new information priority accumulation self-adaptive discrete grey second-order model and its application in electricity generation

Shuangbing Guo, Wenhao Gong, Huanyu Zhou, Dian Li and Yuzhen Chen*

School of Mathematical Sciences, Henan Institute of Science and Technology, Xinxiang 453003, China

* **Correspondence:** Email: chenyuzhen@hist.edu.cn.

Abstract: To effectively capture the nonlinear and complex patterns inherent in small-sample data, this paper proposed a novel self-adaptive second-order discrete grey model incorporating new information priority accumulation. The modeling mechanism and theoretical properties of the proposed model were systematically examined. To mitigate multicollinearity and enhance the stability of parameter estimation in small-sample contexts, Ridge regression regularization was strategically incorporated into the modeling framework. The computational efficiency of the parameter optimization was demonstrated through comparative benchmarking, which substantiated the superiority of the differential evolution algorithm over conventional methods. Furthermore, the model's robustness and stability were verified via Monte Carlo simulations and sensitivity analyses with varying training set proportions. The proposed model was applied to forecast China's total electricity generation as well as generation from specific energy sources. The results demonstrated that the proposed model achieves higher forecasting accuracy than benchmark models. Finally, the power generation across four modes from 2025 to 2030 was predicted and analyzed.

Keywords: discrete grey prediction model; new information priority; self-adaptive; the prediction of electricity generation; Ridge regression regularization

1. Introduction

1.1. Background

In contemporary society, electricity serves not only as an indispensable energy source powering diverse sectors but also as a hallmark of modern civilizational progress. Consequently, rapid global economic expansion and population growth have driven sustained increases in electricity demand. Electricity generation now relies on a broader portfolio of energy sources: conventional fossil fuels (coal and natural gas), nuclear power, and renewable energy including wind, solar, and hydro, alongside emerging energy carriers such as hydrogen. China has undergone rapid economic transformation since 1978,

emerging as a pivotal player in global energy markets [1]. This development, however, has positioned the country as the world's leading carbon dioxide emitter. The growing share of variable renewable energy in the power mix heightens the importance of accurate generation and demand forecasting for energy system optimization and carbon neutrality goals [2]. By advancing sophisticated forecasting methodologies for power generation, we can more effectively balance supply-demand dynamics and integrate renewable resources, ensuring that modern energy systems contribute positively to enhancing global quality of life and environmental sustainability in the forthcoming decades.

At present, various forecasting methods are widely applied in the power generation industry. Grzegorz developed a univariate short-term load forecasting model that integrates linear regression with daily load cycle patterns. This approach enhances forecasting accuracy by streamlining the computational process and mitigating non-stationarity issues [3]. Wang proposed a GA-optimized CNN-LSTM hybrid model that captures spatiotemporal features through heterogeneous network fusion, demonstrating superior predictive capability for photovoltaic power generation [4]. Luo employed historical generation data by calculating mutual information and forming a cluster network structure, thereby building a multi-model deep learning ensemble with varying architectures for accurate photovoltaic power output prediction [5]. Saxena introduced a hyperbolic optimized nonlinear grey model and successfully applied it to market clearing price prediction [6]. Huang advanced grey model initialization theory by incorporating the inverse square root unit (ISRU) function with adjustable parameters as a novel initial condition, thereby demonstrating that nonlinear activation mechanisms enhance derivative-based grey forecasting adaptability. The proposed ISRU-GM(1,1) model accurately predicted electricity consumption trends across Chinese provinces [7].

1.2. Literature review

Whether it be conventional linear regression or advanced deep learning algorithms, they all rely on abundant historical data to reveal hidden patterns within the data. The grey prediction method, derived from grey system theory, exhibits strong universality across diverse situations. It only requires limited historical data to achieve reliable forecasting performance. Therefore, the grey system theory has received increasing attention from scholars and has been employed extensively in various fields. Grey system theory was proposed by Professor Deng in the 1980s as a novel way to investigate the problem of "poor information and uncertainty". The theory extracts valuable information from the generation and development of known data, thereby achieving an accurate description of the system's operational behavior and evolutionary laws [8]. Since the theory was proposed, it has been adopted in many fields, such as agriculture [9], economy [10, 11], energy [12, 13], and transport [14, 15]. Over the past decades, scholars have focused on enhancing the accuracy of grey prediction models and broadening their application scope.

As the basic grey forecasting model, GM(1,1) occasionally fails to fit exponential sequences accurately, owing to the structural inconsistency between its discrete grey differential equation and the continuous whitened response function. To address this limitation, Xie developed the discrete grey model DGM(1,1), which establishes the recursive prediction formula directly from discrete data without relying on continuous whitened equations. Subsequently, Xie proved that this model and the GM(1,1) model are equivalent to each other when the development coefficient of the model is small [16]. Nowadays, discrete grey models have developed into a crucial element of grey system theory. Based on the DGM(1,1) model, Zeng et al. extended the parameter β_2 of the model to $\beta_2 k + \beta_3$, and proposed a non-homogeneous

discrete grey model, which makes the model more adaptable. Subsequently, they proved by mathematical induction that the proposed non-homogeneous model is unbiased for homogeneous exponential curves, non-homogeneous exponential curves, and linear function sequences [17, 18]. To enhance the model's versatility, Luo further extended the parameter β_2 to an Nth-degree polynomial function. The model can be set to a reasonable order N, so that the model can still have a high prediction accuracy in different situations [19]. By introducing fractional-order polynomials, Xu and other scholars proposed a grey prediction model with an optimized grey action quantity, which can search for the optimal order through an intelligent optimization algorithm to ensure the model achieves high prediction accuracy [20]. Ding incorporated Euler polynomials with nonlinear time-varying perturbations into the grey modeling framework, subsequently proposing a Euler polynomial-driven self-adaptive grey prediction model. This formulation enables flexible fitting of diverse curve patterns through adaptive adjustment of the polynomial order [21]. Xia incorporated a structurally adaptive nonlinear correction function into the grey multivariable modeling framework, enabling the model to adjust its structural configuration dynamically in response to varying sample characteristics, thereby substantially enhancing its adaptability [22].

Professor Deng believed that through the accumulation of data, the data without characteristics could show a certain regularity and reduce the randomness of the data. A suitable accumulation operator can reveal latent patterns in raw data. Consequently, scholars have extensively investigated various operators to enhance grey model accuracy. Drawing on exponentially weighted moving average principles, Zhou et al. proposed an adjustable accumulation generation operator. Intelligent optimization of its parameters significantly enhanced the fitting and predictive accuracy of the resulting grey model [23]. Xi proposed a novel prioritized accumulation operator for the GM(1,1) model, emphasizing new information to handle unequally spaced sequences. The model's reliability and applicability were subsequently validated through two case studies [24]. In addition, Wu proposed a fractional-order accumulation operator based on the idea of "in between". This operator can make the model more flexible and accurate [25]. Ma defined the conformable fractional-order accumulation based on the conformable fractional-order derivatives. Subsequently, through a large number of experiments, it was observed that the optimal order of conformable fractional-order accumulation generally ranges between 0 and 1, which is very favorable for algorithmic optimization [26]. In 2020, Wu further proposed the Hausdorff fractional-order accumulation model, which features a simplified accumulation procedure, and demonstrated its independence from initial value selection [27]. Shen integrated the new information priority accumulation operator with the fractional-order accumulation operator, established an improved grey Verhulst model, and further investigated the properties of the integrated operator in detail via Toeplitz matrix theory [13]. Inspired by the forgetting curve phenomenon, Xia formulated an anti-forgetting accumulation generating operator that prioritizes emerging information over historical data, thereby enhancing grey models' adaptability in dynamic systems [28]. Moreover, numerous other scholars have also conducted detailed research on the fractional-order accumulation grey model [29–33].

First-order grey models are typically restricted to a specific data pattern. In contrast, second-order grey models accommodate diverse curve characteristics through variations in the number of real roots of their characteristic equations, thereby exhibiting broader applicability. Since the model was proposed, many scholars have sought to enhance its performance and extend its applicability. Using the original data as modeling data directly, Su proposed a discrete second-order non-homogeneous model, and verified that the model has whitened overlap in different fitting situations [34]. Zeng enhanced

the discrete DGM(2,1) framework by incorporating fractional-order accumulation with exhaustively searched optimal orders, thereby improving prediction accuracy for sequences inadequately handled by conventional second-order grey models [35]. Cheng derived the solution for complex characteristic roots in GM(2,1) and reformulated the grey action quantity as a quadratic polynomial, significantly improving the model's adaptability [36]. Xu and Dang developed a novel gray equation for structural optimization by combining background sequences with inversely accumulated generated sequences. This approach resolves the structural constraints inherent in second-order gray models, thereby establishing a systematic framework for optimizing initial conditions in time-response derivation [37]. Tang avoided the complex construction of background values by proposing the grade difference format. Subsequent parameterization with the goal of minimizing the sum of squared errors greatly improves the model accuracy [38]. Zeng integrated polynomial functions into the DGM(2,1) model and effectively alleviated overfitting issues via regularization techniques [39].

1.3. Summary

Currently, there is relatively little academic attention devoted to the theoretical properties of the second-order grey model. In grey modeling, the evolution of system characteristic data typically exhibits pronounced exponential patterns. However, real-world energy systems rarely follow single exponential trajectories; instead, they commonly undergo distinct developmental phases: incubation, uniform growth, and acceleration [40]. This phenomenon implies that external influences on the system transition from equilibrium to acceleration and subsequently to a new equilibrium state. Consequently, the grey action quantity—representing external system effects—should manifest polynomial rather than monotonic characteristics. This study adopts a quadratic polynomial $ak^2 + bk + c$ as the grey action quantity. Compared with conventional linear formulations, this design enhances model adaptability whilst mitigating overfitting risks associated with higher-order polynomials. To eliminate discretization errors arising from the transition between discrete parameter estimation and continuous prediction, the second-order backward difference operator is employed to transform the differential grey model into its discrete counterpart. Regarding the accumulation mechanism, this study adopts the new information priority accumulated operator proposed in [23], which offers superior operational flexibility and modeling accuracy compared with conventional integer-order accumulation. Moreover, its straightforward inverse reduction formula facilitates direct derivation of the time-response function for the original sequence. Despite recent advances, research on the properties of second-order grey models remains relatively scarce. This paper not only systematically derives the applicable data types for the model under various conditions but also rigorously establishes model unbiasedness. Therefore, this study has both theoretical and practical significance.

Based on the above theory and analysis, this paper establishes a self-adaptive discrete second-order grey model (NIPADGM(2,1)) with new information priority accumulation. The research contributions of this paper are as follows:

1) An adaptive second-order discrete grey model with new information priority accumulation is proposed, and its time-response functions are analytically derived under diverse scenarios.

2) Model unbiasedness is rigorously established for five distinct data types, demonstrating that such unbiasedness is independent of whether the characteristic equation possesses real roots.

3) The introduction of Ridge regression effectively addresses the dual challenges of low parameter-estimation degrees of freedom and prediction instability inherent in second-order grey models under

small-sample conditions.

4) The computational efficiency of the unique algorithm and the robustness of the proposed model are substantiated through comparative performance analysis and Monte Carlo experiments.

5) The theoretical superiority and practical applicability of the proposed framework is substantiated through empirical validation on multi-source power generation systems, demonstrating its capacity to accommodate heterogeneous data characteristics in dynamic forecasting environments.

The rest of the article is presented as follows. Section 2 explains the new model in detail and derives the time-response sequence of the model for different cases. Section 3 demonstrates in detail the uniformity, universality, and unbiasedness of the model. Section 4 verifies the accuracy, effectiveness, and stability of the NIPADGM(2,1) model through multiple sets of experiments. Section 5 applies the model to electricity generation in China. Section 6 summarizes the relevant conclusions of this paper.

2. The NIPADGM(2,1) model

2.1. Construction of the NIPADGM(2,1) model

Definition 1. *[23]: If* $X^{(0)} = \left\{x^{(0)}(1), x^{(0)}(2), \cdots, x^{(0)}(n)\right\}^T$ *is a non-negative original sequence,* $X^{(\alpha)} = \left\{x^{(\alpha)}(1), x^{(\alpha)}(2), \cdots, x^{(\alpha)}(n)\right\}^T$ *is said to be the new information priority accumulation sequence of* α*-order, where*

$$x^{(\alpha)}(k) = \sum_{i=1}^{k} \alpha^{k-i} x^{(0)}(i),\ \alpha \in [0,1], k = 1, 2, \ldots, n. \tag{2.1}$$

If A^α *is a new information priority accumulation generating matrix of* α*-order, then the original data* $X^{(0)}$ *and the accumulated data* $X^{(\alpha)}$ *satisfy the relation* $X^{(\alpha)} = A^\alpha X^{(0)}$*, where*

$$A^\alpha = \begin{bmatrix} 1 & 0 & 0 & \cdots & 0 & 0 \\ \alpha & 1 & 0 & \cdots & 0 & 0 \\ \alpha^2 & \alpha & 1 & \cdots & 0 & 0 \\ \vdots & \vdots & \vdots & & \vdots & \vdots \\ \alpha^{n-2} & \alpha^{n-3} & \alpha^{n-4} & \cdots & 1 & 0 \\ \alpha^{n-1} & \alpha^{n-2} & \alpha^{n-3} & \cdots & \alpha & 1 \end{bmatrix}_{n\times n}.$$

The inverse reduction formula, i.e., Eq (2.2), is derived from the accumulation matrix A^α*.*

$$x^{(0)}(k+1) = x^{(\alpha)}(k+1) - \alpha x^{(\alpha)}(k). \tag{2.2}$$

Using Eq (2.2), we can derive its α*-order reduced matrix* D^α*, and then the original data* $X^{(0)}$ *and the accumulated data* $X^{(\alpha)}$ *satisfy the relation* $X^{(0)} = D^\alpha X^{(\alpha)}$*, where*

$$D^\alpha = \begin{bmatrix} 1 & 0 & 0 & \cdots & 0 & 0 \\ -\alpha & 1 & 0 & \cdots & 0 & 0 \\ 0 & -\alpha & 1 & \cdots & 0 & 0 \\ \vdots & \vdots & \vdots & & \vdots & \vdots \\ 0 & 0 & 0 & \cdots & 1 & 0 \\ 0 & 0 & 0 & \cdots & -\alpha & 1 \end{bmatrix}_{n\times n}.$$

The accumulation matrix A^α and the reduction matrix D^α are inverse to each other, satisfying $A^\alpha D^\alpha = D^\alpha A^\alpha = I$.

Definition 2. *Assuming that $x^{(\alpha)}(k)$ is defined as in Definition 1, the whitened equation of the adaptive second-order grey model with new information priority accumulation (NIPAGM(2,1)) is given as follows:*

$$\frac{d^2x^{(\alpha)}}{dt^2} + a\frac{dx^{(\alpha)}}{dt} + bx^{(\alpha)} = ct^2 + dt + e. \tag{2.3}$$

Replacing $\frac{d^2x^{(\alpha)}}{dt^2}$ with the second-order backward difference $\nabla^2 x^{(\alpha)}(k+1) = x^{(\alpha)}(k+1) - 2x^{(\alpha)}(k) + x^{(\alpha)}(k-1)$, and $\frac{dx^{(\alpha)}}{dt}$ with the first-order backward difference $\nabla x^{(\alpha)}(k+1) = x^{(\alpha)}(k+1) - x^{(\alpha)}(k)$, the whitened equation of the model can be discretized as follows:

$$x^{(\alpha)}(k+1) = \beta_1 x^{(\alpha)}(k) + \beta_2 x^{(\alpha)}(k-1) + \beta_3 k^2 + \beta_4 k + \beta_5, \tag{2.4}$$

where $\beta_1 = \frac{2+a}{1+a+b}$, $\beta_2 = \frac{-1}{1+a+b}$, $\beta_3 = \frac{c}{1+a+b}$, $\beta_4 = \frac{2c+d}{1+a+b}$, $\beta_5 = \frac{c+d+e}{1+a+b}$. At this point, the NIPAGM(2,1) model is transformed into an adaptive second-order discrete grey model with new information priority accumulation, hereafter abbreviated as NIPADGM(2,1), where $\theta = [\beta_1, \beta_2, \beta_3, \beta_4, \beta_5]^T$ is the parameter vector of the model.

Theorem 1. *Assuming that $x^{(\alpha)}(k)$ and $x^{(\alpha)}(k)$ are as described in Definition 1, the parameter vector $\theta = [\beta_1, \beta_2, \cdots, \beta_5]^T$ of the NIPADGM(1,1) model can be expressed as*

$$\theta = (B^T B)^{-1} B^T Y, \tag{2.5}$$

where

$$B = \begin{pmatrix} x^{(\alpha)}(2) & x^{(\alpha)}(1) & 2^2 & 2 & 1 \\ x^{(\alpha)}(3) & x^{(\alpha)}(2) & 3^2 & 3 & 1 \\ \vdots & \vdots & \vdots & \vdots & \vdots \\ x^{(\alpha)}(n-1) & x^{(\alpha)}(n-2) & (n-1)^2 & n-1 & 1 \end{pmatrix}, Y = \begin{pmatrix} x^{(\alpha)}(3) \\ x^{(\alpha)}(4) \\ \vdots \\ x^{(\alpha)}(n) \end{pmatrix}.$$

Proof. By setting the value of k to take values from 2 to $n-1$ in sequence, we can obtain the following set of equations:

$$\begin{cases} x^{(\alpha)}(3) = x^{(\alpha)}(2)\beta_1 + x^{(\alpha)}(1)\beta_2 + 2^2\beta_3 + 2\beta_4 + \beta_5, \\ x^{(\alpha)}(4) = x^{(\alpha)}(3)\beta_1 + x^{(\alpha)}(2)\beta_2 + 3^2\beta_3 + 3\beta_4 + \beta_5, \\ \quad \vdots \\ x^{(\alpha)}(n) = x^{(\alpha)}(n-1)\beta_1 + x^{(\alpha)}(n-2)\beta_2 + (n-1)^2\beta_3 + (n-1)\beta_4 + \beta_5. \end{cases} \tag{2.6}$$

The above system of equations can be transformed into the following form:

$$Y = \begin{pmatrix} x^{(\alpha)}(3) \\ x^{(\alpha)}(4) \\ \vdots \\ x^{(\alpha)}(n) \end{pmatrix} = B\theta = \begin{pmatrix} x^{(\alpha)}(2) & x^{(\alpha)}(1) & 2^2 & 2 & 1 \\ x^{(\alpha)}(3) & x^{(\alpha)}(2) & 3^2 & 3 & 1 \\ \vdots & \vdots & \vdots & \vdots & \vdots \\ x^{(\alpha)}(n-1) & x^{(\alpha)}(n-2) & (n-1)^2 & n-1 & 1 \end{pmatrix} \begin{pmatrix} \beta_1 \\ \beta_2 \\ \beta_3 \\ \beta_4 \\ \beta_5 \end{pmatrix}, \text{ where } B \text{ is an } (n-2)\times 5$$

matrix. When $n > 7$, Eq (2.6) becomes an overdetermined system of equations. In this case, there is no exact solution. Its matrix form is $Y = B\theta$, and then the error sequence is $\varepsilon = (\varepsilon_1, \varepsilon_2, \cdots, \varepsilon_n) = Y - B\theta$.

If the sum of squares of the error sequence is minimized, the result of Eq (2.7) is minimized.

$$\begin{aligned}\varepsilon^2 &= \varepsilon^T\varepsilon \\ &= (Y - B\theta)^T (Y - B\theta) \\ &= \sum_{k=2}^{n}\left[\beta_1 x^{(\alpha)}(k) + \beta_2 x^{(\alpha)}(k-1) + \beta_3 k^2 + \beta_4 k + \beta_5 - x^{(\alpha)}(k+1)\right]^2.\end{aligned} \tag{2.7}$$

According to Fermat's theorem, we have

$$\frac{d\varepsilon^2}{d\theta} = 2B^T B\theta - 2B^T Y = 0. \tag{2.8}$$

By organizing the system of differential equations, we obtain

$$\theta = (\beta_1, \beta_2, \cdots, \beta_5)^T = (B^T B)^{-1} B^T Y. \tag{2.9}$$

□

Theorem 2. *If θ, B, Y are as shown in Theorem 1, when the condition ${\beta_1}^2 + 4\beta_2 > 0$ holds, λ_1 and λ_2 are unequal real roots of the model characteristic equation. Then the time-response sequences of the model at this time have the following two expressions.*

(1) If $\lambda_1 \neq 1$ and $\lambda_2 \neq 1$, then the time-response sequence of the model is

$$\begin{aligned}\hat{x}^{(0)}(k+1) = (\lambda_1 - \alpha)\hat{\phi}_1{\lambda_1}^{k-1} + (\lambda_2 - \alpha)\hat{\phi}_2{\lambda_2}^{k-1} + (1-\alpha)\hat{\phi}_3 k^2 + \\ [2\alpha\hat{\phi}_3 + (1-\alpha)\hat{\phi}_4]k + [-\alpha\hat{\phi}_3 + \alpha\hat{\phi}_4 + (1-\alpha)\hat{\phi}_5],\end{aligned} \tag{2.10}$$

where

$$\begin{cases}\hat{\phi}_1 = x^{(\alpha)}(1) + \frac{1}{\lambda_1-\lambda_2}[x^{(\alpha)}(2) - \lambda_1 x^{(\alpha)}(1) + \frac{\beta_3+\beta_4+\beta_5}{\lambda_2-1} + \frac{\lambda_2(\beta_3+\beta_4)}{(\lambda_2-1)^2} + \frac{2\lambda_2{}^2\beta_3}{(\lambda_2-1)^3}] \\ \quad -\frac{1}{\lambda_1-1}[\frac{\beta_5}{\lambda_2-1} + \frac{\lambda_2\beta_4}{(\lambda_2-1)^2} + \frac{\lambda_2(\lambda_2+1)\beta_3}{(\lambda_2-1)^3} + \frac{\lambda_1(\beta_4-\beta_3)}{(\lambda_1-1)(\lambda_2-1)} + \frac{2\lambda_1(2\lambda_1\lambda_2-\lambda_1-\lambda_2)\beta_3}{(\lambda_1-1)^2(\lambda_2-1)^2}], \\ \hat{\phi}_2 = \frac{1}{\lambda_2-\lambda_1}[x^{(\alpha)}(2) - \lambda_1 x^{(\alpha)}(1) + \frac{\beta_3+\beta_4+\beta_5}{\lambda_2-1} + \frac{\lambda_2(\beta_3+\beta_4)}{(\lambda_2-1)^2} + \frac{2\lambda_2{}^2\beta_3}{(\lambda_2-1)^3}], \\ \hat{\phi}_3 = \frac{\beta_3}{(\lambda_1-1)(\lambda_2-1)}, \\ \hat{\phi}_4 = \frac{\beta_4}{(\lambda_1-1)(\lambda_2-1)} + \frac{2\lambda_2\beta_3}{(\lambda_1-1)(\lambda_2-1)^2} + \frac{2\lambda_1\beta_3}{(\lambda_1-1)^2(\lambda_2-1)}, \\ \hat{\phi}_5 = \frac{1}{\lambda_1-1}[\frac{\beta_5}{\lambda_2-1} + \frac{\lambda_2\beta_4}{(\lambda_2-1)^2} + \frac{\lambda_2\beta_3(\lambda_2+1)}{(\lambda_2-1)^3} + \frac{\lambda_1(\beta_4-\beta_3)}{(\lambda_1-1)(\lambda_2-1)} + \frac{2\lambda_1(2\lambda_1\lambda_2-\lambda_1-\lambda_2)\beta_3}{(\lambda_1-1)^2(\lambda_2-1)^2}].\end{cases}$$

(2) When the value of one of the characteristic roots of λ_1 and λ_2 is 1, we set the condition $\lambda_1 \neq 1, \lambda_2 = 1$, and the time-response sequence of the model at this time is

$$\begin{aligned}\hat{x}^{(0)}(k+1) = (\lambda_1 - \alpha)\hat{\phi}_1{\lambda_1}^{k-1} + (1-\alpha)\hat{\phi}_2 k^3 + [3\alpha\hat{\phi}_2 + (1-\alpha)\hat{\phi}_3]k^2 \\ + [-3\alpha\hat{\phi}_2 + 2\alpha\hat{\phi}_3 + (1-\alpha)\hat{\phi}_4]k + [\alpha\hat{\phi}_2 - \alpha\hat{\phi}_3 + \alpha\hat{\phi}_4 \\ + (1-\alpha)\hat{\phi}_5],\end{aligned} \tag{2.11}$$

where

$$\begin{cases}\hat{\phi}_1 = \frac{x^{(\alpha)}(2)-x^{(\alpha)}(1)}{\lambda_1-1} - \frac{\beta_3+\beta_4+\beta_5}{\lambda_1-1} + \frac{\lambda_1\beta_5}{(\lambda_1-1)^2} + \frac{\lambda_1{}^2\beta_4}{(\lambda_1-1)^3} + \frac{\lambda_1{}^2(\lambda_1+1)\beta_3}{(\lambda_1-1)^4}, \\ \hat{\phi}_2 = -\frac{\beta_3}{3(\lambda_1-1)}, \\ \hat{\phi}_3 = -[\frac{\beta_3+\beta_4}{2(\lambda_1-1)} + \frac{\lambda_1\beta_3}{(\lambda_1-1)^2}], \\ \hat{\phi}_4 = -[\frac{1}{(\lambda_1-1)}(\frac{\beta_3}{6} + \frac{\beta_4}{2} + \beta_5) + \frac{\lambda_1\beta_4}{(\lambda_1-1)^2} + \frac{\lambda_1(\lambda_1+1)\beta_3}{(\lambda_1-1)^3}], \\ \hat{\phi}_5 = -[\frac{x^{(\alpha)}(2)-\lambda_1 x^{(\alpha)}(1)}{\lambda_1-1} - \frac{\beta_3+\beta_4+\beta_5}{\lambda_1-1} + \frac{\lambda_1\beta_5}{(\lambda_1-1)^2} + \frac{\lambda_1{}^2\beta_4}{(\lambda_1-1)^3} + \frac{\lambda_1{}^2(\lambda_1+1)\beta_3}{(\lambda_1-1)^4}].\end{cases}$$

Proof. From the basic form of the model, the characteristic equation of the model is

$$\lambda^2 - \beta_1\lambda - \beta_2 = 0. \tag{2.12}$$

Since ${\beta_1}^2 + 4\beta_2 > 0$, there are two unequal real roots of the Eq (2.12). Let λ_1 and λ_2 be the two real roots of Eq (2.12), so we have

$$\lambda_1 = \frac{\beta_1 + \sqrt{{\beta_1}^2 + 4\beta_2}}{2}, \tag{2.13}$$

$$\lambda_2 = \frac{\beta_1 - \sqrt{{\beta_1}^2 + 4\beta_2}}{2}. \tag{2.14}$$

From Vedda's theorem, $\lambda_1 + \lambda_2 = \beta_1$ and $\lambda_1\lambda_2 = -\beta_2$. Bringing the two characteristic roots into the basic form of the model, Eq (2.4) can be modified into

$$x^{(\alpha)}(k+1) - \lambda_1 x^{(\alpha)}(k) = \lambda_2(x^{(\alpha)}(k) - \lambda_1 x^{(\alpha)}(k-1)) + \beta_3 k^2 + \beta_4 k + \beta_5. \tag{2.15}$$

Let $y^{(\alpha)}(k) = x^{(\alpha)}(k+1) - \lambda_1 x^{(\alpha)}(k)$. Then, Eq (2.15) can be further converted into

$$y^{(\alpha)}(k) = \lambda_2 y^{(\alpha)}(k-1) + \beta_3 k^2 + \beta_4 k + \beta_5. \tag{2.16}$$

At this point, the basic form of the model is successfully downgraded from a second-order difference equation to a first-order difference equation.

(1) When $\lambda_1 \neq 1$ and $\lambda_2 \neq 1$, Eq (2.16) can be converted to

$$\begin{aligned} &y^{(\alpha)}(k) + \frac{\beta_3}{\lambda_2 - 1}k^2 + [\frac{\beta_4}{\lambda_2 - 1} + \frac{2\lambda_2\beta_3}{(\lambda_2 - 1)^2}]k \\ &+ [\frac{\beta_5}{\lambda_2 - 1} + \frac{\lambda_2\beta_4}{(\lambda_2 - 1)^2} + \frac{\lambda_2(\lambda_2 + 1)\beta_3}{(\lambda_2 - 1)^3}] \\ &= \lambda_2[y^{(\alpha)}(k-1) + \frac{\beta_3}{\lambda_2 - 1}(k-1)^2 + (\frac{\beta_4}{\lambda_2 - 1} + \frac{2\lambda_2\beta_3}{(\lambda_2 - 1)^2})(k-1) \\ &+ \frac{\beta_5}{\lambda_2 - 1} + \frac{\lambda_2\beta_4}{(\lambda_2 - 1)^2} + \frac{\lambda_2(\lambda_2 + 1)\beta_3}{(\lambda_2 - 1)^3}]. \end{aligned} \tag{2.17}$$

Let $z^{(\alpha)}(k) = y^{(\alpha)}(k) + \frac{\beta_3}{\lambda_2 - 1}k^2 + [\frac{\beta_4}{\lambda_2 - 1} + \frac{2\lambda_2\beta_3}{(\lambda_2 - 1)^2}]k + [\frac{\beta_5}{\lambda_2 - 1} + \frac{\lambda_2\beta_4}{(\lambda_2 - 1)^2} + \frac{\lambda_2(\lambda_2 + 1)\beta_3}{(\lambda_2 - 1)^3}]$, and at this point there is $z^{(\alpha)}(k) = \lambda_2 z^{(\alpha)}(k-1)$ holds. From the definition of a geometric sequence, the sequence $z^{(\alpha)}(k)$ is a geometric sequence with $z^{(\alpha)}(1)$ as the first term and λ_2 as the common ratio. $z^{(\alpha)}(1)$ can be calculated by

$$\begin{aligned} z^{(\alpha)}(1) &= y^{(\alpha)}(1) + \frac{\beta_3}{\lambda_2 - 1} + \frac{\beta_4}{\lambda_2 - 1} + \frac{2\lambda_2\beta_3}{\lambda_2 - 1^2} + \frac{\beta_5}{\lambda_2 - 1} \\ &\quad + \frac{\lambda_2\beta_4}{(\lambda_2 - 1)^2} + \frac{\lambda_2(\lambda_2 + 1)}{(\lambda_2 - 1)^3} \\ &= y^{(\alpha)}(1) + \frac{\beta_3 + \beta_4 + \beta_5}{\lambda_2 - 1} + \frac{\lambda_2(\beta_3 + \beta_4)}{(\lambda_2 - 1)^2} + \frac{2{\lambda_2}^2\beta_3}{(\lambda_2 - 1)^3}. \end{aligned} \tag{2.18}$$

From the properties of the geometric sequence, it can be seen that $z^{(\alpha)}(k) = z^{(\alpha)}(1){\lambda_2}^{k-1}$. Therefore,

$$\begin{aligned} & y^{(\alpha)}(k) + \frac{\beta_3}{\lambda_2 - 1}k^2 + [\frac{\beta_4}{\lambda_2 - 1} + \frac{2\lambda_2\beta_3}{(\lambda_2 - 1)^2}]k \\ & + [\frac{\beta_5}{\lambda_2 - 1} + \frac{\lambda_2\beta_4}{(\lambda_2 - 1)^2} + \frac{\lambda_2(\lambda_2 + 1)\beta_3}{(\lambda_2 - 1)^3}] \\ & = [y^{(\alpha)}(1) + \frac{\beta_3 + \beta_4 + \beta_5}{\lambda_2 - 1} + \frac{\lambda_2(\beta_3 + \beta_4)}{(\lambda_2 - 1)^2} + \frac{2{\lambda_2}^2\beta_3}{(\lambda_2 - 1)^3}]{\lambda_2}^{k-1}. \end{aligned} \tag{2.19}$$

Equation (2.20) can be obtained by collating Eq (2.19) and substituting $x^{(\alpha)}(k+1) - \lambda_1 x^{(\alpha)}(k)$ for $y^{(\alpha)}(k)$.

$$x^{(\alpha)}(k+1) - \lambda_1 x^{(\alpha)}(k) = \zeta_1{\lambda_2}^{k-1} + \zeta_2 k^2 + \zeta_3 k + \zeta_4, \tag{2.20}$$

where $\zeta_1 = x^{(\alpha)}(2) - \lambda_1 x^{(\alpha)}(1) + \frac{\beta_3+\beta_4+\beta_5}{\lambda_2-1} + \frac{\lambda_2(\beta_3+\beta_4)}{(\lambda_2-1)^2} + \frac{2{\lambda_2}^2\beta_3}{(\lambda_2-1)^3}$, $\zeta_2 = -\frac{\beta_3}{\lambda_2-1}$, $\zeta_3 = -[\frac{\beta_4}{\lambda_2-1} + \frac{2\lambda_2\beta_3}{(\lambda_2-1)^2}]$, $\zeta_4 = -[\frac{\beta_5}{\lambda_2-1} + \frac{\lambda_2\beta_4}{(\lambda_2-1)^2} + \frac{\lambda_2(\lambda_2+1)\beta_3}{(\lambda_2-1)^3}]$.

At this point, Eq (2.20) can be converted into

$$\begin{aligned} & x^{(\alpha)}(k+1) + \frac{\zeta_1}{\lambda_1 - \lambda_2}{\lambda_2}^k + \frac{\zeta_2}{\lambda_1 - 1}k^2 + (\frac{\zeta_3}{\lambda_1 - 1} \\ & + \frac{2\lambda_1\zeta_2}{(\lambda_1 - 1)^2})k + \frac{\zeta_4}{\lambda_1 - 1} + \frac{\lambda_1(\zeta_3 - \zeta_2)}{(\lambda_1 - 1)^2} + \frac{2{\lambda_1}^2\zeta_2}{(\lambda_1 - 1)^3} \\ & = \lambda_1[x^{(\alpha)}(k) + \frac{\zeta_1}{\lambda_1 - \lambda_2}{\lambda_2}^{k-1} + \frac{\zeta_2}{\lambda_1 - 1}(k-1)^2 + (\frac{\zeta_3}{\lambda_1 - 1} \\ & + \frac{2\lambda_1\zeta_2}{(\lambda_1 - 1)^2})(k-1) + \frac{\zeta_4}{\lambda_1 - 1} + \frac{\lambda_1(\zeta_3 - \zeta_2)}{(\lambda_1 - 1)^2} + \frac{2{\lambda_1}^2\zeta_2}{(\lambda_1 - 1)^3}]. \end{aligned} \tag{2.21}$$

Let $w^{(\alpha)}(k+1) = x^{(\alpha)}(k+1) + \frac{\zeta_1}{\lambda_1-\lambda_2}{\lambda_2}^k + \frac{\zeta_2}{\lambda_1-1}k^2 + (\frac{\zeta_3}{\lambda_1-1} + \frac{2\lambda_1\zeta_2}{(\lambda_1-1)^2})k + \frac{\zeta_4}{\lambda_1-1} + \frac{\lambda_1(\zeta_3-\zeta_2)}{(\lambda_1-1)^2} + \frac{2{\lambda_1}^2\zeta_2}{(\lambda_1-1)^3}$.

In this case, we have $w^{(\alpha)}(k+1) = \lambda_1 w^{(\alpha)}(k)$. Therefore, the sequence $w^{(\alpha)}(k)$ is a geometric sequence with $w^{(\alpha)}(1)$ as the first term and λ_1 as the common ratio. $w^{(\alpha)}(1)$ can be calculated by

$$w^{(\alpha)}(1) = x^{(\alpha)}(1) + \frac{\zeta_1}{\lambda_1 - \lambda_2} + \frac{\zeta_4}{\lambda_1 - 1} + \frac{\lambda_1(\zeta_3 - \zeta_2)}{(\lambda_1 - 1)^2} + \frac{2{\lambda_1}^2\zeta_2}{(\lambda_1 - 1)^3}. \tag{2.22}$$

From the properties of the geometric sequence, there is a formula $w^{(\alpha)}(k+1) = {\lambda_1}^k w^{(\alpha)}(1)$ that holds. Therefore,

$$\begin{aligned} & x^{(\alpha)}(k+1) + \frac{\zeta_1}{\lambda_1 - \lambda_2}{\lambda_2}^k + \frac{\zeta_2}{\lambda_1 - 1}k^2 + (\frac{\zeta_3}{\lambda_1 - 1} + \frac{2\lambda_1\zeta_2}{(\lambda_1 - 1)^2})k \\ & + \frac{\zeta_4}{\lambda_1 - 1} + \frac{\lambda_1(\zeta_3 - \zeta_2)}{(\lambda_1 - 1)^2} + \frac{2{\lambda_1}^2\zeta_2}{(\lambda_1 - 1)^3} \\ & = [x^{(\alpha)}(1) + \frac{\zeta_1}{\lambda_1 - \lambda_2} + \frac{\zeta_4}{\lambda_1 - 1} + \frac{\lambda_1(\zeta_3 - \zeta_2)}{(\lambda_1 - 1)^2} + \frac{2{\lambda_1}^2\zeta_2}{(\lambda_1 - 1)^3}]{\lambda_1}^k. \end{aligned} \tag{2.23}$$

By collapsing, we obtain that

$$\hat{x}^{(\alpha)}(k+1) = \hat{\phi}_1{\lambda_1}^k + \hat{\phi}_2{\lambda_2}^k + \hat{\phi}_3 k^2 + \hat{\phi}_4 k + \hat{\phi}_5, \tag{2.24}$$

where

$$\begin{cases}\hat{\phi}_1 = x^{(\alpha)}(1) + \frac{1}{\lambda_1-\lambda_2}[x^{(\alpha)}(2) - \lambda_1 x^{(\alpha)}(1) + \frac{\beta_3+\beta_4+\beta_5}{\lambda_2-1} + \frac{\lambda_2(\beta_3+\beta_4)}{(\lambda_2-1)^2} + \frac{2\lambda_2{}^2\beta_3}{(\lambda_2-1)^3}] \\ \quad - \frac{1}{\lambda_1-1}[\frac{\beta_5}{\lambda_2-1} + \frac{\lambda_2\beta_4}{(\lambda_2-1)^2} + \frac{\lambda_2(\lambda_2+1)\beta_3}{(\lambda_2-1)^3} + \frac{\lambda_1(\beta_4-\beta_3)}{(\lambda_1-1)(\lambda_2-1)} + \frac{2\lambda_1(2\lambda_1\lambda_2-\lambda_1-\lambda_2)\beta_3}{(\lambda_1-1)^2(\lambda_2-1)^2}], \\ \hat{\phi}_2 = \frac{1}{\lambda_2-\lambda_1}[x^{(\alpha)}(2) - \lambda_1 x^{(\alpha)}(1) + \frac{\beta_3+\beta_4+\beta_5}{\lambda_2-1} + \frac{\lambda_2(\beta_3+\beta_4)}{(\lambda_2-1)^2} + \frac{2\lambda_2{}^2\beta_3}{(\lambda_2-1)^3}], \\ \hat{\phi}_3 = \frac{\beta_3}{(\lambda_1-1)(\lambda_2-1)}, \\ \hat{\phi}_4 = \frac{\beta_4}{(\lambda_1-1)(\lambda_2-1)} + \frac{2\lambda_2\beta_3}{(\lambda_1-1)(\lambda_2-1)^2} + \frac{2\lambda_1\beta_3}{(\lambda_1-1)^2(\lambda_2-1)}, \\ \hat{\phi}_5 = \frac{1}{\lambda_1-1}[\frac{\beta_5}{\lambda_2-1} + \frac{\lambda_2\beta_4}{(\lambda_2-1)^2} + \frac{\lambda_2\beta_3(\lambda_2+1)}{(\lambda_2-1)^3} + \frac{\lambda_1(\beta_4-\beta_3)}{(\lambda_1-1)(\lambda_2-1)} + \frac{2\lambda_1(2\lambda_1\lambda_2-\lambda_1-\lambda_2)\beta_3}{(\lambda_1-1)^2(\lambda_2-1)^2}].\end{cases}$$

Based on Eq (2.2), we can obtain that

$$\begin{aligned}\hat{x}^{(0)}(k+1) &= \hat{x}^{(\alpha)}(k+1) - \alpha\hat{x}^{(\alpha)}(k) \\ &= \hat{\phi}_1{\lambda_1}^k + \hat{\phi}_2{\lambda_2}^k + \hat{\phi}_3k^2 + \hat{\phi}_4k + \hat{\phi}_5 - \alpha[\hat{\phi}_1{\lambda_1}^{k-1} \\ &\quad + \hat{\phi}_2{\lambda_2}^{k-1} + \hat{\phi}_3(k-1)^2 + \hat{\phi}_4(k-1) + \hat{\phi}_5] \\ &= (\lambda_1-\alpha)\hat{\phi}_1{\lambda_1}^{k-1} + (\lambda_2-\alpha)\hat{\phi}_2{\lambda_2}^{k-1} + (1-\alpha)\hat{\phi}_3k^2 + [2\alpha\hat{\phi}_3 + (1-\alpha)\hat{\phi}_4]k \\ &\quad + [-\alpha\hat{\phi}_3 + \alpha\hat{\phi}_4 + (1-\alpha)\hat{\phi}_5].\end{aligned}$$

(2) When the value of one of the characteristic roots is 1, the model derivation steps are similar to those in the first case, as they both involve constructing a geometric sequence to solve for the time-response sequences of the model. Therefore, it will not be developed in detail here. □

Theorem 3. *If θ, B, and Y are as shown in Theorem 1, when ${\beta_1}^2 + 4\beta_2 = 0$, λ_1 and λ_2 are two equal real roots of the characteristic equation of the model, and then the time-response sequences of the model at this time have the following three expressions.*

(1) When $\lambda_1 = \lambda_2 = 0$, the time-response sequence of the model is

$$\hat{x}^{(0)}(k+1) = (1-\alpha)\beta_3k^2 + [2\alpha\beta_3 + (1-\alpha)\beta_4]k + [\alpha(-\beta_3+\beta_4) + (1-\alpha)\beta_5]. \tag{2.25}$$

(2) When $\lambda_1 = \lambda_2 = 1$, the time-response sequence of the model is

$$\begin{aligned}\hat{x}^{(0)}(k+1) =& (1-\alpha)\hat{\phi}_1k^4 + [4\alpha\hat{\phi}_1 + (1-\alpha)\hat{\phi}_2]k^3 + [-6\alpha\hat{\phi}_1 + 3\alpha\hat{\phi}_2 \\ &+ (1-\alpha)\hat{\phi}_3]k^2 + [4\alpha\hat{\phi}_1 - 3\alpha\hat{\phi}_2 + 2\alpha\hat{\phi}_3 + (1-\alpha)\hat{\phi}_4]k \\ &+ [\alpha(-\hat{\phi}_1 + \hat{\phi}_2 - \hat{\phi}_3 + \hat{\phi}_4) + (1-\alpha)\hat{\phi}_5],\end{aligned} \tag{2.26}$$

where $\hat{\phi}_1 = \frac{\beta_3}{12}, \hat{\phi}_2 = \frac{\beta_3}{3} + \frac{\beta_4}{6}, \hat{\phi}_3 = \frac{5}{12}\beta_3 + \frac{\beta_4}{2} + \frac{\beta_5}{2}, \hat{\phi}_4 = x^{(\alpha)}(2) - x^{(\alpha)}(1) - \frac{5}{6}\beta_3 - \frac{2}{3}\beta_4 - \frac{\beta_5}{2}, \hat{\phi}_5 = x^{(\alpha)}(1)$.

(3) When $\lambda_1 = \lambda_2 = \lambda$, λ is neither equal to 0 nor equal to 1, and the time-response sequence of the model is

$$\begin{aligned}\hat{x}^{(0)}(k+1) =& [(\lambda-\alpha)\hat{\phi}_1 + \alpha\hat{\phi}_2 + (\lambda-\alpha)\hat{\phi}_2k]\lambda^{k-1} + (1-\alpha)\hat{\phi}_3k^2 \\ &+ [2\alpha\hat{\phi}_3 + (1-\alpha)\hat{\phi}_4]k + [-\alpha(\hat{\phi}_3 - \hat{\phi}_4) + (1-\alpha)\hat{\phi}_5],\end{aligned} \tag{2.27}$$

where $\hat{\phi}_1 = x^{(\alpha)}(1) - \frac{\beta_5}{(\lambda-1)^2} + \frac{2\lambda(\beta_3-\beta_4)}{(\lambda-1)^3} - \frac{6\lambda^2\beta_3}{(\lambda-1)^4}, \hat{\phi}_2 = \frac{1}{\lambda}[x^{(\alpha)}(2) - x^{(\alpha)}(1) + \frac{\beta_3+\beta_4+\beta_5}{\lambda-1} + \frac{\lambda(\beta_3+\beta_4)}{(\lambda-1)^2} + \frac{2\lambda^2\beta_3}{(\lambda-1)^3}]$, $\hat{\phi}_3 = \frac{\beta_3}{(\lambda-1)^2}$, $\hat{\phi}_4 = \frac{\beta_4}{(\lambda-1)^2} + \frac{4\lambda\beta_3}{(\lambda-1)^3}, \hat{\phi}_5 = \frac{\beta_5}{(\lambda-1)^2} + \frac{2\lambda(\beta_4-\beta_3)}{(\lambda-1)^3} + \frac{6\lambda^2\beta_3}{(\lambda-1)^4}$.

The idea of the proof is similar to that of Theorem 2, so it will not be developed in detail here.

Theorem 4. *If θ, B, and Y are as shown in Theorem 1, the characteristic equation of the model has no real roots when ${\beta_1}^2 + 4\beta_2 < 0$. In this case, the time-response sequence of the original model data is expressed as*

$$\hat{x}^{(0)}(k+1) = \rho^k[D\cos k\theta + E\sin k\theta] + Fk^2 + Gk + H, \tag{2.28}$$

where $\rho = \sqrt{-\beta_2}$, $\theta = \arctan\frac{\sqrt{-\Delta}}{\beta_1}$, $\Delta = {\beta_1}^2 + 4\beta_2$, $D = p(\rho\cos\theta - \alpha) + q\rho\sin\theta$, $E = -p\rho\sin\theta + q(\rho\cos\theta - \alpha)$, $F = (1-\alpha)A$, $G = 2A + (1-\alpha)B$, $H = A + B + (1-\alpha)C$, $A = \frac{\beta_3}{1-\beta_2-\beta_3}$, $B = \frac{-2(1+\beta_2)\beta_3}{(\beta_1+\beta_2-1)^2} - \frac{\beta_4}{\beta_1+\beta_2-1}$, $C = -\frac{2(1+\beta_2)^2\beta_3}{(\beta_1+\beta_2-1)^3} - \frac{(1+\beta_2)\beta_4}{(\beta_1+\beta_2-1)^2} + \frac{(\beta_2-1)\beta_3}{(\beta_1+\beta_2-1)^2} - \frac{\beta_5}{\beta_1+\beta_2-1}$, $p = \frac{[x^{(\alpha)}(1)-A-B-C](-\beta_2)^{\frac{1}{2}(n-1)}\sin(n\arctan\frac{\sqrt{-\Delta}}{\beta_1}) - [x^{(\alpha)}(n)-An^2-Bn-C]\sin(\arctan\frac{\sqrt{-\Delta}}{\beta_1})}{\sin[(n-1)\arctan\frac{\sqrt{-\Delta}}{\beta_1}](-\beta_2)^{\frac{1}{2}n}}$, $q = \frac{[x^{(\alpha)}(n)-An^2-Bn-C]\cos(\arctan\frac{\sqrt{-\Delta}}{\beta_1}) - [x^{(\alpha)}(1)-A-B-C](-\beta_2)^{\frac{1}{2}(n-1)}\cos(n\arctan\frac{\sqrt{-\Delta}}{\beta_1})}{\sin[(n-1)\arctan\frac{\sqrt{-\Delta}}{\beta_1}](-\beta_2)^{\frac{1}{2}n}}$.

Proof. When ${\beta_1}^2 + 4\beta_2 < 0$, the model is essentially a second-order non-homogeneous difference equation. The general solution of the Eq (2.4) is equal to the summation of the general solution of the homogeneous second-order difference equation and the special solution of the non-homogeneous second-order difference equation. Since the non-homogeneous terms in Eq (2.4) are quadratic polynomials, the particular solution of the non-homogeneous second-order difference equation is also a quadratic polynomial.

Let the special solution of the model be $\hat{x}_q^{(\alpha)}(k+1) = A(k+1)^2 + B(k+1) + C$, and we bring this special solution into Eq (2.4) to get

$$\begin{aligned} A(k+1)^2 + B(k+1) + C =& \beta_1[Ak^2 + Bk + C] + \beta_2[A(k-1)^2 \\ &+ B(k-1) + C] + \beta_3k^2 + \beta_4k + \beta_5. \end{aligned} \tag{2.29}$$

Solve for $A = \frac{\beta_3}{1-\beta_2-\beta_3}$, $B = \frac{-2(1+\beta_2)\beta_3}{(\beta_1+\beta_2-1)^2} - \frac{\beta_4}{\beta_1+\beta_2-1}$, $C = -\frac{2(1+\beta_2)^2\beta_3}{(\beta_1+\beta_2-1)^3} - \frac{(1+\beta_2)\beta_4}{(\beta_1+\beta_2-1)^2} + \frac{(\beta_2-1)\beta_3}{(\beta_1+\beta_2-1)^2} - \frac{\beta_5}{\beta_1+\beta_2-1}$.

The homogeneous equation for this model is

$$x^{(\alpha)}(k+1) = \beta_1x^{(\alpha)}(k) + \beta_2x^{(\alpha)}(k-1). \tag{2.30}$$

Therefore, the general solution of this homogeneous equation is

$$\begin{aligned} \hat{x}_p^{(\alpha)}(k+1) =& (-\beta_2)^{\frac{1}{2}(k+1)}[p\cos((k+1)\arctan\frac{\sqrt{-\Delta}}{\beta_1}) \\ &+ q\sin((k+1)\arctan\frac{\sqrt{-\Delta}}{\beta_1})], \end{aligned} \tag{2.31}$$

where p and q are the model parameters [39]. At this moment, the general solution of the model can be formulated as

$$\begin{aligned} \hat{x}^{(\alpha)}(k+1) =& \hat{x}_p^{(\alpha)}(k+1) + \hat{x}_q^{(\alpha)}(k+1) \\ =& (-\beta_2)^{\frac{1}{2}(k+1)}\{p\cos[(k+1)\arctan\frac{\sqrt{-\Delta}}{\beta_1}] + q\sin[(k \\ &+ 1)\arctan\frac{\sqrt{-\Delta}}{\beta_1}]\} + A(k+1)^2 + B(k+1) + C. \end{aligned} \tag{2.32}$$

To solve for the parameters, the following initial conditions are set up.

$$\hat{x}^{(\alpha)}(1) = x^{(\alpha)}(1), \hat{x}^{(\alpha)}(n) = x^{(\alpha)}(n). \tag{2.33}$$

When $k = 0$,

$$x^{(\alpha)}(1) = (-\beta_2)^{\frac{1}{2}}[p\cos(\arctan\frac{\sqrt{-\Delta}}{\beta_1}) + q\sin(\arctan\frac{\sqrt{-\Delta}}{\beta_1})] + A + B + C. \tag{2.34}$$

When $k = n - 1$,

$$\begin{aligned} x^{(\alpha)}(n) = (-\beta_2)^{\frac{1}{2}n}[p\cos(n\arctan\frac{\sqrt{-\Delta}}{\beta_1}) + q\sin(n\arctan\frac{\sqrt{-\Delta}}{\beta_1})] \\ + An^2 + Bn + C. \end{aligned} \tag{2.35}$$

By manipulating Eqs (2.34) and (2.35), we can obtain

$$\begin{pmatrix} \cos(\arctan\frac{\sqrt{-\Delta}}{\beta_1}) & \sin(\arctan\frac{\sqrt{-\Delta}}{\beta_1}) \\ \cos(n\arctan\frac{\sqrt{-\Delta}}{\beta_1}) & \sin(n\arctan\frac{\sqrt{-\Delta}}{\beta_1}) \end{pmatrix}\begin{pmatrix} p \\ q \end{pmatrix} = \begin{pmatrix} [x^{(\alpha)}(1) - A - B - C](-\beta_2)^{-\frac{1}{2}} \\ [x^{(\alpha)}(n) - An^2 - Bn - C](-\beta_2)^{-\frac{1}{2}n} \end{pmatrix}.$$

The parameters p and q can be found using Cramer's rule, where

$$p = \frac{[x^{(\alpha)}(1) - A - B - C](-\beta_2)^{\frac{1}{2}(n-1)}\sin(n\arctan\frac{\sqrt{-\Delta}}{\beta_1}) - [x^{(\alpha)}(n) - An^2 - Bn - C]\sin(\arctan\frac{\sqrt{-\Delta}}{\beta_1})}{\sin[(n-1)\arctan\frac{\sqrt{-\Delta}}{\beta_1}](-\beta_2)^{\frac{1}{2}n}},$$

$$q = \frac{[x^{(\alpha)}(n) - An^2 - Bn - C]\cos(\arctan\frac{\sqrt{-\Delta}}{\beta_1}) - [x^{(\alpha)}(1) - A - B - C](-\beta_2)^{\frac{1}{2}(n-1)}\cos(n\arctan\frac{\sqrt{-\Delta}}{\beta_1})}{\sin[(n-1)\arctan\frac{\sqrt{-\Delta}}{\beta_1}](-\beta_2)^{\frac{1}{2}n}}.$$

Upon determining the parameters involved in $\hat{x}^{(\alpha)}(k+1)$, let $\rho = \sqrt{-\beta_2}$ and $\theta = \arctan\frac{\sqrt{-\Delta}}{\beta_1}$, whereupon Eq (2.32) can be transformed into

$$\hat{x}^{(\alpha)}(k+1) = \rho^{k+1}[p\cos((k+1)\theta) + q\sin((k+1)\theta)] + A(k+1)^2 + B(k+1) + C. \tag{2.36}$$

The restored value of the model is obtained through Eq (2.2) as follows:

$$\begin{aligned} \hat{x}^{(0)}(k+1) &= \hat{x}^{(\alpha)}(k+1) - \alpha\hat{x}^{(\alpha)}(k) \\ &= \rho^{k+1}[p\cos((k+1)\theta) + q\sin((k+1)\theta)] + A(k+1)^2 + B(k+1) + C \\ &\quad - \alpha\{\rho^k[p\cos(k\theta) + q\sin(k\theta)] + Ak^2 + Bk + C\} \\ &= \rho^k[D\cos k\theta + E\sin k\theta] + Fk^2 + Gk + H, \end{aligned} \tag{2.37}$$

where $D = p(\rho\cos\theta - \alpha) + q\rho\sin\theta$, $E = -p\rho\sin\theta + q(\rho\cos\theta - \alpha)$, $F = (1-\alpha)A$, $G = 2A + (1-\alpha)B$, $H = A + B + (1-\alpha)C$. □

2.2. Determination of the model hyperparameter

The determination of the model time-response sequence mainly depends on the model structure parameter vector θ, and the calculation of θ is closely related to the model hyperparameter α. Therefore, a reasonable hyperparameter can effectively improve model accuracy. In this paper, under the objective of minimizing the mean absolute percentage error between the fitted data and the actual data, we construct an objective function for the hyperparameter α, which is given by Eq (2.38).

$$fitness = \min_{\alpha} \ MAPE = \frac{1}{n-1}\sum_{k=2}^{n}\left|\frac{\hat{x}^{(0)}(k) - x^{(0)}(k)}{x^{(0)}(k)}\right| \times 100\%. \tag{2.38}$$

The above optimization problem aims to find the optimal hyperparameter α. However, traditional mathematical methods have difficult calculating the optimal solution when faced with highly complex and nonlinear optimization problems. Therefore, this paper uses the differential evolution optimization algorithm to solve for the model hyperparameter vector. Differential evolution (DE) is a classical evolutionary optimization algorithm proposed by Storn and Price in 1995. It simulates the mutation, crossover, and selection mechanisms of natural evolution, iteratively optimizes the individuals in the population, and is mainly employed to solve global optimization problems in continuous search spaces [41]. Due to its excellent characteristics such as strong global search capabilities and good robustness, this algorithm can effectively solve high-latitude, nonlinear optimization problems and has been widely applied in many fields such as agriculture, engineering, artificial intelligence, and image processing. The flowchart of the NIPADGM(2,1) model is illustrated in Figure 1.

2.3. Model evaluation metrics

In terms of the indexes to test the model's merits, this paper selects three common model evaluation indexes as the criteria for assessing the model's performance from multiple perspectives, namely, absolute percentage error *(APE)*, mean absolute percentage error *(MAPE)*, and root mean squared error *(RMSE)*. The equations are as described below.

$$APE = \left|\frac{\hat{x}^{(0)}(k) - x^{(0)}(k)}{x^{(0)}(k)}\right| \times 100\%. \tag{2.39}$$

$$MAPE = \frac{1}{n-1}\sum_{k=2}^{n}\left|\frac{\hat{x}^{(0)}(k) - x^{(0)}(k)}{x^{(0)}(k)}\right| \times 100\%. \tag{2.40}$$

$$RMSE = \sqrt{\frac{1}{n-1}\sum_{k=2}^{n}\left(\hat{x}^{(0)}(k) - x^{(0)}(k)\right)^2}. \tag{2.41}$$

In addition, *MAPEsim, MAPEpre*, and *MAPEtot* represent the mean absolute percentage error of the model on the training set, validation set, and training and validation sets combined, respectively. *RMSEsim, RMSEpre*, and *RMSEtot* represent the root mean square error of the model on the training set, validation set, and training and validation sets combined, respectively.

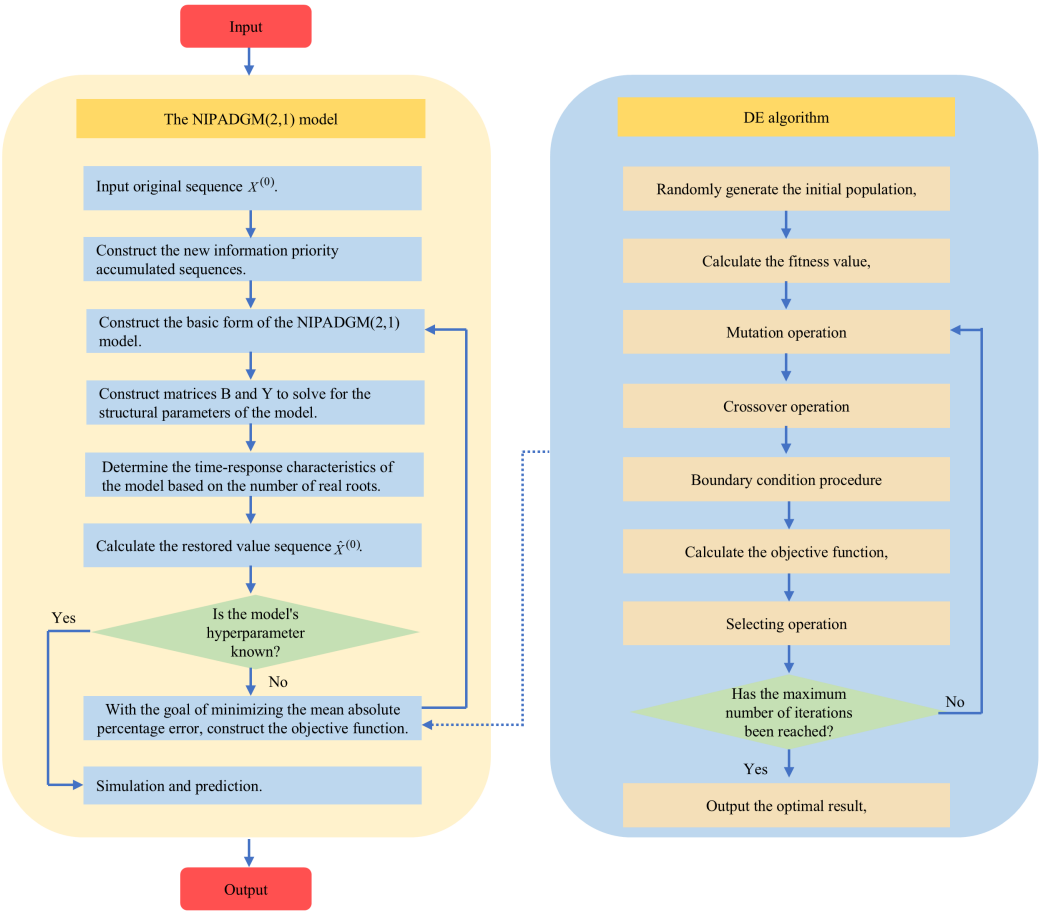

Figure 1. The flowchart of the NIPADGM(2,1) model.

3. Model properties

3.1. The compatibility of the NIPADGM(2,1) model

Property 1: The model has compatibility. Many of the existing grey models are special cases of this model.

(1) When $\beta_2 = \beta_3 = \beta_4 = 0$ and $\alpha = 1$, the NIPADGM(2,1) model is reduced into the DGM(1,1) model [16]. The DGM(1,1) model is particularly suited for fitting non-homogeneous exponentially growing data, such as the GDP.

(2) When $\beta_2 = \beta_3 = 0$ and $\alpha = 1$, the NIPADGM(2,1) model is changed to the NDGM(1,1) model [18]. In the literature, the NDGM(1,1) model was applied to forecast solar power generation.

(3) When $\beta_2 = 0$ and $\alpha = 1$, the NIPADGM(2,1) model is transformed into the DGMP(1,1,2) model [19]. The DGMP(1,1,2) is particularly suited for modeling data sequences exhibiting partial exponential patterns combined with polynomial characteristics, and has been applied to energy demand forecasting in case studies.

(4) When $\beta_2 = \beta_3 = \beta_4 = 0$, the NIPADGM(2,1) model is reduced to the NIPDGM(1,1) model [23]. In the literature, the NIPDGM(1,1) model was applied to forecast energy consumption.

(5) When $\beta_3 = 0$ and $\alpha = 0$, the NIPADGM(2,1) model is transformed into the DNDGM(2,1)

model [34]. In the literature, the DNDGM(2,1) model has been applied to forecast per capita energy consumption.

(6) When $\beta_3 = \beta_4 = 0$ and $\alpha = 1$, the NIPADGM(2,1) model is changed to the DGM(2,1) model [42]. In the literature, this model has been applied to the prediction of residential electricity consumption.

3.2. The universality of the NIPADGM(2,1) model

Property 2: The model can fit a variety of different curves, with a certain degree of universality.

(1) When $\lambda_1 \neq \lambda_2$, and neither of the two real roots is equal to 1, then $\hat{x}^{(0)}(k+1) = (\lambda_1 - \alpha)\phi_1{\lambda_1}^{k-1} + (\lambda_2 - \alpha)\phi_2{\lambda_2}^{k-1} + (1-\alpha)\phi_3 k^2 + [2\alpha\phi_3 + (1-\alpha)\phi_4]k + [-\alpha\phi_3 + \alpha\phi_4 + (1-\alpha)\phi_5]$. Since λ_1, λ_2, and α are real numbers, the model restored value $\hat{x}^{(0)}(k+1)$ can be regarded as the result of the summation of a sequence of quadratic functions and two sequences of exponential functions with different bases in this case.

(2) When $\lambda_1 \neq \lambda_2$, and one of the two real roots is 1, for example, $\lambda_1 \neq 1$ and $\lambda_2 = 1$, $\hat{x}^{(0)}(k+1) = (\lambda_1 - \alpha)\phi_1{\lambda_1}^{k-1} + (1-\alpha)\phi_2 k^3 + [3\alpha\phi_2 + (1-\alpha)\phi_3]k^2 + [-3\alpha\phi_2 + 2\alpha\phi_3 + (1-\alpha)\phi_4]k + [\alpha\phi_2 - \alpha\phi_3 + \alpha\phi_4 + (1-\alpha)\phi_5]$. Since λ_1 and α are real numbers, the model restored value $\hat{x}^{(0)}(k+1)$ can be regarded as the result of the summation of a sequence of cubic functions and sequences of exponential functions in this case.

(3) When $\lambda_1 = \lambda_2 = 1$, $\hat{x}^{(0)}(k+1) = (1-\alpha)\phi_1 k^4 + [4\alpha\phi_1 + (1-\alpha)\phi_2]k^3 + [-6\alpha\phi_1 + 3\alpha\phi_2 + (1-\alpha)\phi_3]k^2 + [4\alpha\phi_1 - 3\alpha\phi_2 + 2\alpha\phi_3 + (1-\alpha)\phi_4]k + [\alpha(-\phi_1 + \phi_2 - \phi_3 + \phi_4) + (1-\alpha)\phi_5]$. Since α is a real number, the model restored value $\hat{x}^{(0)}(k+1)$ can be regarded as a power function sequence with degrees not exceeding four in this case.

(4) When $\lambda_1 = \lambda_2 = \lambda$, and λ is neither equal to 0 nor equal to 1, then $\hat{x}^{(0)}(k+1) = [(\lambda - \alpha)\phi_1 + \alpha\phi_2 + (\lambda - \alpha)\phi_2 k]\lambda^{k-1} + (1-\alpha)\phi_3 k^2 + [2\alpha\phi_3 + (1-\alpha)\phi_4]k + [-\alpha(\phi_3 - \phi_4) + (1-\alpha)\phi_5]$. Since λ and α are real numbers, the model restored value $\hat{x}^{(0)}(k+1)$ can be regarded as the summation of a product sequence of a linear sequence and an exponential sequence, and another quadratic function sequence in this case.

(5) When ${\beta_1}^2 + 4\beta_2 < 0$, the characteristic equation of the model has no real roots. In this case, $\hat{x}^{(0)}(k+1) = \rho^k[D\cos k\theta + E\sin k\theta] + Fk^2 + Gk + H$. Since ρ, D, E, F, G and H are real numbers, the model restored value $\hat{x}^{(0)}(k+1)$ can be regarded as the sum of two components: the product of an exponential function and a linear combination of trigonometric functions, and a quadratic polynomial.

Corollary 1. *When $\lambda_1 \in (-1,1), \lambda_2 \in (-1,1)$, $\lambda_1 \neq \lambda_2$ and $\beta_3 = \beta_4 = 0$, there exists a convergence value of the model's time-response sequence, i.e.,* $\lim\limits_{k\to\infty} x^{(0)}(k) = x^* = \frac{(1-\alpha)\beta_5}{1-\beta_1-\beta_2}$.

Proof. When $\lambda_1 \in (-1,1), \lambda_2 \in (-1,1)$, $\lambda_1 \neq \lambda_2$ and $\beta_3 = \beta_4 = 0$, the time-response sequence of the model at this point is $\hat{x}^{(0)}(k+1) = (\lambda_1 - \alpha)\phi_1{\lambda_1}^{k-1} + (\lambda_2 - \alpha)\phi_2{\lambda_2}^{k-1} + (1-\alpha)\phi_5$, where $\phi_5 = \frac{\beta_5}{(\lambda_1-1)(\lambda_2-1)}$.

Since $\lambda_1 \in (-1,1), \lambda_2 \in (-1,1)$, α, ϕ_1, and ϕ_2 are real numbers, the following equation holds:

$\lim\limits_{k\to\infty} (\lambda_1 - \alpha)\phi_1{\lambda_1}^{k-1} = 0$, $\lim\limits_{k\to\infty} (\lambda_2 - \alpha)\phi_2{\lambda_2}^{k-1} = 0$.

Therefore, $\lim\limits_{k\to\infty} x^{(0)}(k) = (1-\alpha)\phi_5 = \frac{(1-\alpha)\beta_5}{1-(\lambda_1+\lambda_2)+\lambda_1\lambda_2} = \frac{(1-\alpha)\beta_5}{1-\beta_1-\beta_2}$. □

Corollary 2. *When $\lambda_1 = \lambda_2 = \lambda, \lambda \in (-1,1)$, and $\beta_3 = \beta_4 = 0$, there exists a convergence value of the model's time-response sequence, i.e.,* $\lim\limits_{k\to\infty} x^{(0)}(k) = x^* = \frac{4(1-\alpha)\beta_5}{(\beta_1-2)^2}$.

The proof is similar to Corollary 1 and will not be developed in detail here.

3.3. The unbiasedness of the NIPADGM(2,1) model

Property 3: When the original data $X^{(0)}$ follows the distribution $x^{(0)}(k+1) = \phi_1{\lambda_1}^k + \phi_2{\lambda_2}^k + \phi_3k^2 + \phi_4k + \phi_5$, the model is unbiased for this type of data.

Proof. When the characteristic equation has two real roots that are both not equal to 1, the α-order accumulation sequence $X^{(\alpha)}$ follows the distribution

$$\begin{aligned}
&\phi_1{\lambda_1}^k + \phi_2{\lambda_2}^k + \phi_3k^2 + \phi_4k + \phi_5\\
&= (\lambda_1+\lambda_2)[\phi_1{\lambda_1}^{k-1} + \phi_2{\lambda_2}^{k-1} + \phi_3(k-1)^2 + \phi_4(k-1) + \phi_5]\\
&\quad - \lambda_1\lambda_2[\phi_1{\lambda_1}^{k-2} + \phi_2{\lambda_2}^{k-2} + \phi_3(k-2)^2 + \phi_4(k-2) + \phi_5]\\
&\quad + (\lambda_1-1)(\lambda_2-1)\phi_3k^2 + [(\lambda_1-1)(\lambda_2-1)\phi_4 + 2(\lambda_1+\lambda_2\\
&\quad - 2\lambda_1\lambda_2)\phi_3]k + (\lambda_1-1)(\lambda_2-1)\phi_5 + (\lambda_1+\lambda_2-2\lambda_1\lambda_2)\phi_4\\
&\quad + (4\lambda_1\lambda_2 - \lambda_1 - \lambda_2)\phi_3.
\end{aligned} \tag{3.1}$$

Therefore, $\beta_1 = \lambda_1+\lambda_2, \beta_2 = -\lambda_1\lambda_2, \beta_3 = (\lambda_1-1)(\lambda_2-1)\phi_3, \beta_4 = (\lambda_1-1)(\lambda_2-1)\phi_4 + 2(\lambda_1+\lambda_2-2\lambda_1\lambda_2)\phi_3, \beta_5 = (\lambda_1-1)(\lambda_2-1)\phi_5 + (\lambda_1+\lambda_2-2\lambda_1\lambda_2)\phi_4 + (4\lambda_1\lambda_2-\lambda_1-\lambda_2)\phi_3$ are the exact solutions of the system of equations in Theorem 1, and thus the results of the calculations of Eq (2.4). Bringing β_1, $\beta_2, \beta_3, \beta_4, \beta_5$ into the prediction equation of the model, Eq (2.10), the following equation holds.

$$\begin{aligned}
\hat{\phi}_2 &= \frac{1}{\lambda_2-\lambda_1}[x^{(\alpha)}(2) - \lambda_1x^{(\alpha)}(1) + \frac{\beta_3+\beta_4+\beta_5}{\lambda_2-1} + \frac{\lambda_2(\beta_3+\beta_4)}{(\lambda_2-1)^2} + \frac{2{\lambda_2}^2\beta_3}{(\lambda_2-1)^3}]\\
&= \frac{1}{\lambda_2-\lambda_1}[\phi_1\lambda_1 + \phi_2\lambda_2 + \phi_3 + \phi_4 + \phi_5 - \lambda_1(\phi_1+\phi_2+\phi_5) + \frac{\beta_3}{\lambda_2-1}\\
&\quad + \frac{\lambda_2\beta_3}{(\lambda_2-1)^2} + \frac{2{\lambda_2}^2\beta_3}{(\lambda_2-1)^3} + \frac{\beta_4}{\lambda_2-1} + \frac{\lambda_2\beta_4}{(\lambda_2-1)^2} + \frac{\beta_5}{\lambda_2-1}]\\
&= \frac{1}{\lambda_2-\lambda_1}[(\lambda_2-\lambda_1)\phi_2 + \phi_3 + \phi_4 + (1-\lambda_1)\phi_5\\
&\quad + \frac{4{\lambda_2}^2 - 3\lambda_2 + 1}{(\lambda_2-1)^3}\beta_3 + \frac{2\lambda_2-1}{(\lambda_2-1)^2}\beta_4 + \frac{1}{\lambda_2-1}\beta_5]\\
&= \frac{1}{\lambda_2-\lambda_1}[(\lambda_2-\lambda_1)\phi_2 + \phi_3 + \phi_4 + (1-\lambda_1)\phi_5 + \frac{(4{\lambda_2}^2 - 3\lambda_2 + 1)(\lambda_1-1)(\lambda_2-1)\phi_3}{(\lambda_2-1)^3}\\
&\quad + \frac{(2\lambda_2-1)[(\lambda_1-1)(\lambda_2-1)\phi_4 + 2(\lambda_1+\lambda_2-2\lambda_1\lambda_2)\phi_3]}{(\lambda_2-1)^2}\\
&\quad + \frac{(\lambda_1-1)(\lambda_2-1)\phi_5 + (\lambda_1+\lambda_2-2\lambda_1\lambda_2)\phi_4 + (4\lambda_1\lambda_2-\lambda_1-\lambda_2)\phi_3}{\lambda_2-1}] = \phi_2.
\end{aligned} \tag{3.2}$$

Similarly, the following equation holds.

$$\hat{\phi}_3 = \frac{(\lambda_1-1)(\lambda_2-1)\phi_3}{(\lambda_1-1)(\lambda_2-1)} = \phi_3. \tag{3.3}$$

$$\begin{aligned}\hat{\phi}_4 = &\frac{(\lambda_1-1)(\lambda_2-1)\phi_4 + 2(\lambda_1+\lambda_2-2\lambda_1\lambda_2)\phi_3}{(\lambda_1-1)(\lambda_2-1)} + \frac{2\lambda_2(\lambda_1-1)(\lambda_2-1)\phi_3}{(\lambda_1-1)(\lambda_2-1)^2} \\ &+ \frac{2\lambda_1(\lambda_1-1)(\lambda_2-1)\phi_3}{(\lambda_1-1)^2(\lambda_2-1)} = \phi_4.\end{aligned} \tag{3.4}$$

$$\begin{aligned}\hat{\phi}_5 = &\frac{1}{\lambda_1-1}[\frac{(\lambda_1-1)(\lambda_2-1)\phi_5 + (\lambda_1+\lambda_2-2\lambda_1\lambda_2)\phi_4 + (4\lambda_1\lambda_2-\lambda_1-\lambda_2)\phi_3}{\lambda_2-1} \\ &+ \frac{\lambda_2[(\lambda_1-1)(\lambda_2-1)\phi_4 + 2(\lambda_1+\lambda_2-2\lambda_1\lambda_2)\phi_3]}{(\lambda_2-1)^2} + \frac{\lambda_2(\lambda_2+1)(\lambda_1-1)(\lambda_2-1)\phi_3}{(\lambda_2-1)^3} \\ &+ \frac{\lambda_1[(\lambda_1-1)(\lambda_2-1)\phi_4 + 2(\lambda_1+\lambda_2-2\lambda_1\lambda_2)\phi_3]}{(\lambda_1-1)(\lambda_2-1)} - \frac{\lambda_1(\lambda_1-1)(\lambda_2-1)\phi_3}{(\lambda_1-1)(\lambda_2-1)} \\ &+ \frac{2\lambda_1(2\lambda_1\lambda_2-\lambda_1-\lambda_2)(\lambda_1-1)(\lambda_2-1)\phi_3}{(\lambda_1-1)^2(\lambda_2-1)^2}] = \phi_5.\end{aligned} \tag{3.5}$$

In the case that the initial condition $\hat{x}^{(\alpha)}(1) = x^{(\alpha)}(1)$ holds, then $\hat{\phi}_1 + \hat{\phi}_2 + \hat{\phi}_5 = \phi_1 + \phi_2 + \phi_5$ holds. $\hat{\phi}_1 = (\phi_1 + \phi_2 + \phi_5) - (\hat{\phi}_2 + \hat{\phi}_5) = \phi_1$.

In summary, we have proved that the time-response sequences $X^{(\alpha)}$ and $\hat{X}^{(\alpha)}$ are identical, so the restored value $\hat{X}^{(0)}$ must be identical to the original value $X^{(0)}$. In this case, there is only a calculation error in the model, and there is no error in the model itself. Since the new information priority accumulation does not change the data type, the model is also unbiased when the original data $X^{(0)}$ obeys the $x^{(0)}(k+1) = \phi_1{\lambda_1}^k + \phi_2{\lambda_2}^k + \phi_3k^2 + \phi_4k + \phi_5$ distribution. □

Based on the proof of Property 3, Properties 4–7 can also be derived.

Property 4: When the original data $X^{(0)}$ follows the distribution $\hat{x}^{(0)}(k+1) = \phi_1{\lambda_1}^k + \phi_2k^3 + \phi_3k^2 + \phi_4k + \phi_5$, the model is unbiased for this type of data.

Property 5: When the original data $X^{(0)}$ follows the distribution $\hat{x}^{(0)}(k+1) = \phi_1k^4+\phi_2k^3+\phi_3k^2+\phi_4k+\phi_5$, the model is unbiased for this type of data.

Property 6: When the original data $X^{(0)}$ follows the distribution $\hat{x}^{(0)}(k+1) = (\phi_1 + \phi_2k)\lambda^k + \phi_3k^2 + \phi_4k + \phi_5$, the model is unbiased for this type of data.

Property 7: When the original data $X^{(0)}$ follows the distribution $\hat{x}^{(0)}(k+1) = \rho^{k+1}[p\cos((k+1)\theta) + q\sin((k+1)\theta)] + A(k+1)^2 + B(k+1) + C$, the model is unbiased for this type of data.

Proof: When ${\beta_1}^2 + 4\beta_2 < 0$, the original data is accumulated by α-order and follows the distribution $\hat{x}^{(\alpha)}(k+1) = \rho^{k+1}[p\cos((k+1)\theta) + q\sin((k+1)\theta)] + A(k+1)^2 + B(k+1) + C$. Employing Euler's formula, Eq (2.36) is converted to the following form:

$$\begin{aligned}\hat{x}^{(\alpha)}(k+1) &= \rho^{k+1}[p\cos((k+1)\theta) + q\sin((k+1)\theta)] + A(k+1)^2 + B(k+1) + C \\ &= \rho^{k+1}\left[p\frac{e^{i(k+1)\theta} + e^{-i(k+1)\theta}}{2} + q\frac{e^{i(k+1)\theta} - e^{-i(k+1)\theta}}{2i}\right] + A(k+1)^2 + B(k+1) + C \\ &= \frac{p-qi}{2}[re^{i\theta}]^{k+1} + \frac{p+qi}{2}[re^{-i\theta}]^{k+1} + A(k+1)^2 + B(k+1) + C \\ &= \varphi_1{\lambda_1}^k + \varphi_2{\lambda_2}^k + \varphi_3k^2 + \varphi_4k + \varphi_5,\end{aligned} \tag{3.6}$$

where $\lambda_1 = \rho e^{i\theta}$, $\lambda_2 = \rho e^{-i\theta}$, $\varphi_1 = \frac{p-qi}{2}\lambda_1$, $\varphi_2 = \frac{p+qi}{2}\lambda_2$, $\varphi_3 = A$, $\varphi_4 = 2A + B$, $\varphi_5 = A + B + C$. φ_1, φ_2 are complex conjugates. λ_1, λ_2 are the complex roots of the characteristic equation, satisfying $\lambda_1 + \lambda_2 = \beta_1$ and $\lambda_1\lambda_2 = -\beta_2$. The subsequent proof process is similar to that of Property 3 and will not be repeated here.

Properties 3–7 show that if $X^{(\alpha)}$ strictly follows the above five curve function distributions, the data $\hat{X}^{(\alpha)}$ is exactly the same as the actual data $X^{(\alpha)}$. Therefore, the restored value $\hat{X}^{(0)}$ obtained by $\hat{X}^{(\alpha)}$ after the α-order reducible reduction must be exactly the same as $X^{(0)}$. In this case, there is only a calculation error in the model, and there is no error in the model itself. Since the new information priority accumulation of α-order does not change the data type, in other words, the model is also unbiased when the original data $X^{(0)}$ obeys the five curve distributions described in Properties 3–7.

3.4. The case study of model unbiasedness

In Properties 3–7, this paper illustrates that the model is theoretically unbiased for the above five types of data. In this section, we will use five real-world cases to verify the simulation, each of which uses 10 data volumes.

The five sets of data sequences are designed to be modeled separately, and the expressions of the five sets of data are as follows.

$X_1 = \left(x_1{}^{(0)}(1), x_1{}^{(0)}(2), \cdots, x_1{}^{(0)}(k)\right)$, where $x_1{}^{(0)}(k) = 0.4 \times 1.4^k + 0.6 \times 1.9^k + 2k^2 + k + 1$.

$X_2 = \left(x_2{}^{(0)}(1), x_2{}^{(0)}(2), \cdots, x_2{}^{(0)}(k)\right)$, where $x_2{}^{(0)}(k) = 1.4 \times 2^k + 0.7k^3 + 0.8k^2 + k + 1$.

$X_3 = \left(x_3{}^{(0)}(1), x_3{}^{(0)}(2), \cdots, x_3{}^{(0)}(k)\right)$, where $x_3{}^{(0)}(k) = k^4 + 2k^3 + 3k^2 + 4k + 5$.

$X_4 = \left(x_4{}^{(0)}(1), x_4{}^{(0)}(2), \cdots, x_4{}^{(0)}(k)\right)$, where $x_4{}^{(0)}(k) = (0.2 + 0.4k) \times 1.1^k + 2k^2 + k + 1$.

$X_5 = \left(x_5{}^{(0)}(1), x_5{}^{(0)}(2), \cdots, x_5{}^{(0)}(k)\right)$, where $x_5{}^{(0)}(k) = 1.2^k \times \left[3\cos\frac{\pi}{4}k + 4\sin\frac{\pi}{3}k\right] + 2k^2 + 3k + 4$.

Let the parameter k be taken from 1 to 10 in turn, and the five sets of data are modeled separately. At the same time, GMP(1,1,N) [19], FHGM(1,1) [27], GM(1,1) [8], and DGM(1,1) [16] are utilized as comparison models. The calculation results are recorded in Table 1 and Figure 2.

Table 1. Model fitting results under different curves.

		NIPADGM(2,1)		GMP(1,1,N)		FHGM(1,1)		GM(1,1)		DGM(1,1)	
Group 1											
Number	Actual value	Values	*APE (%)*	Values	*APE (%)*	Values	*APE (%)*	Values	*APE (%)*	Values	*APE (%)*
1	5.70	5.70	0.00%	5.70	0.00%	5.70	0.00%	5.70	0.00%	5.70	0.00%
2	13.95	13.95	0.00%	20.25	45.15%	19.46	39.47%	19.46	39.48%	19.8579	42.35%
3	27.21	27.21	0.00%	30.52	12.13%	29.67	9.01%	29.67	9.02%	30.4705	11.97%
4	46.36	46.36	0.00%	46.20	0.34%	45.23	2.42%	45.23	2.42%	46.7548	0.86%
5	73.01	73.01	0.00%	70.15	3.91%	68.97	5.53%	68.97	5.53%	71.7418	1.73%
6	110.24	110.24	0.00%	106.74	3.17%	105.16	4.61%	105.16	4.61%	110.0825	0.14%
7	163.85	163.85	0.00%	162.64	0.74%	160.33	2.15%	160.33	2.15%	168.9136	3.09%
8	244.80	244.80	0.00%	248.02	1.31%	244.46	0.14%	244.46	0.14%	259.1856	5.87%
9	373.88	373.88	0.00%	378.43	1.22%	372.73	0.31%	372.74	0.31%	397.7014	6.37%
10	590.43	590.44	0.00%	577.63	2.17%	568.31	3.75%	568.32	3.75%	610.2438	3.36%
			0.00%		7.79%		7.49%		7.49%		8.42%
Group 2											
Number	Actual value	Values	*APE (%)*	values	*APE (%)*	Values	*APE (%)*	Values	*APE (%)*	Values	*APE (%)*
1	6.30	6.30	0.00%	6.30	0.00%	6.30	0.00%	6.30	0.00%	6.30	0.00%

Continued on the next page

Table 1 – continued from the previous page

		Values	*APE (%)*	Values	*APE (%)*	Values	*APE (%)*	Values	*APE (%)*	Values	*APE (%)*
2	17.40	17.40	0.00%	23.31	33.99%	25.06	44.02%	43.32	148.99%	44.69	156.84%
3	41.30	41.30	0.00%	47.52	15.07%	49.60	20.10%	72.67	75.95%	75.86	83.68%
4	85.00	85.00	0.00%	87.67	3.14%	90.84	6.87%	121.89	43.40%	128.78	51.50%
5	158.30	158.30	0.00%	154.25	2.56%	160.42	1.34%	204.44	29.15%	218.60	38.09%
6	276.60	276.60	0.00%	264.65	4.32%	277.32	0.26%	342.91	23.97%	371.07	34.15%
7	466.50	466.50	0.00%	447.74	4.02%	472.67	1.32%	575.17	23.30%	629.88	35.02%
8	777.00	777.00	0.00%	751.37	3.30%	797.62	2.65%	964.75	24.16%	1069.23	37.61%
9	1301.90	1301.90	0.00%	1254.88	3.61%	1335.93	2.61%	1618.19	24.29%	1815.01	39.41%
10	2224.60	2224.60	0.00%	2089.87	6.06%	2224.60	0.00%	2714.21	22.01%	3080.99	38.50%
			0.00%		8.45%		8.80%		46.14%		57.20%

Group 3

Number	Actual value	Values	*APE (%)*	Values	*APE (%)*	Values	*APE (%)*	Values	*APE (%)*	Values	*APE (%)*
1	15	15.00	0.00%	15.00	0.00%	15.00	0.00%	15.00	0.00%	15.00	0.00%
2	57.00	57.00	0.00%	54.90	3.68%	147.64	159.01%	572.29	904.02%	594.70	943.34%
3	179.00	179.00	0.00%	178.75	0.14%	357.62	99.79%	910.12	408.45%	952.86	432.33%
4	453.00	453.00	0.00%	446.66	1.40%	714.19	57.66%	1447.36	219.51%	1526.72	237.02%
5	975.00	975.00	0.00%	962.16	1.32%	1304.64	33.81%	2301.75	136.08%	2446.18	150.89%
6	1865.00	1865.00	0.00%	1845.94	1.02%	2262.51	21.31%	3660.49	96.27%	3919.37	110.15%
7	3267.00	3267.00	0.00%	3238.71	0.87%	3791.71	16.06%	5821.29	78.18%	6279.79	92.22%
8	5349.00	5349.00	0.00%	5304.47	0.83%	6202.26	15.95%	9257.63	73.07%	10,061.76	88.11%
9	8303.00	8303.00	0.00%	8234.40	0.83%	9963.31	20.00%	14,722.46	77.31%	16,121.39	94.16%
10	12345.00	12345.00	0.00%	12251.38	0.76%	15,781.97	27.84%	23,413.20	89.66%	25,830.40	109.24%
			0.00%		1.20%		50.16%		231.39%		250.83%

Group 4

Number	Actual value	Values	*APE (%)*	Values	*APE (%)*	Values	*APE (%)*	Values	*APE (%)*	Values	*APE (%)*
1	4.66	4.66	0.00%	4.66	0.00%	4.66	0.00%	4.66	0.00%	4.66	0.00%
2	12.21	12.21	0.00%	12.20	0.06%	13.06	6.95%	29.43	141.02%	29.87	144.66%
3	23.86	23.86	0.00%	23.86	0.01%	25.23	5.72%	38.63	61.90%	39.25	64.49%
4	39.64	39.64	0.00%	39.63	0.02%	40.18	1.39%	50.72	27.96%	51.58	30.12%
5	59.54	59.54	0.00%	59.53	0.02%	58.55	1.67%	66.58	11.83%	67.77	13.81%
6	83.61	83.61	0.00%	83.59	0.02%	80.98	3.14%	87.41	4.55%	89.04	6.50%
7	111.85	111.85	0.00%	111.83	0.01%	108.25	3.22%	114.76	2.60%	117.00	4.61%
8	144.29	144.29	0.00%	144.28	0.01%	141.22	2.12%	150.65	4.41%	153.73	6.54%
9	180.96	180.96	0.00%	180.95	0.01%	180.94	0.01%	197.78	9.29%	201.99	11.62%
10	221.89	221.89	0.00%	221.87	0.01%	228.59	3.02%	259.64	17.01%	265.41	19.61%
			0.00%		0.02%		3.03%		31.18%		33.55%

Group 5

Number	Actual value	Values	*APE (%)*	Values	*APE (%)*	Values	*APE (%)*	Values	*APE (%)*	Values	*APE (%)*
1	15.70	15.70	0.00%	15.70	0.02%	15.70	0.02%	15.70	0.02%	15.70	0.02%
2	22.99	22.99	0.00%	26.52	15.37%	38.88	69.14%	38.88	69.14%	40.24	75.05%
3	27.33	27.34	0.01%	21.75	20.44%	49.70	81.83%	49.70	81.83%	51.32	87.75%
4	34.60	34.57	0.08%	33.36	3.58%	63.53	83.64%	63.53	83.64%	65.45	89.17%
5	55.10	55.14	0.06%	58.92	6.93%	81.21	47.39%	81.21	47.39%	83.46	51.47%
6	94.00	94.03	0.03%	94.95	1.01%	103.81	10.44%	103.81	10.44%	106.44	13.24%
7	143.01	142.97	0.02%	136.48	4.57%	132.70	7.21%	132.70	7.21%	135.74	5.08%
8	183.79	183.79	0.00%	176.37	4.04%	169.63	7.70%	169.63	7.70%	173.11	5.81%
9	203.95	203.92	0.01%	204.42	0.23%	216.84	6.32%	216.84	6.32%	220.77	8.25%
10	212.55	212.55	0.00%	206.05	3.06%	277.18	30.41%	277.18	30.41%	281.55	32.46%
			0.02%		5.92%		34.41%		34.41%		36.83%

Table 1 shows that the NIPADGM(2,1) model achieves a perfect fit for all data types, with the

absolute percentage error being 0% at most time points. At certain time points in Case 5, the error did not reach 0%, which may be due to computational errors introduced during the model's processing. From Figure 2, it can be visualized that the NIPADGM(2,1) model outperforms the comparative models when facing different types of data. Therefore, when the data sequences strictly satisfy the distribution of these five data types, the NIPADGM(2,1) model can achieve perfect fitting. The NIPADGM(2,1) model can also achieve high fitting accuracy when the data sequences approximately satisfy the distribution of these five data types.

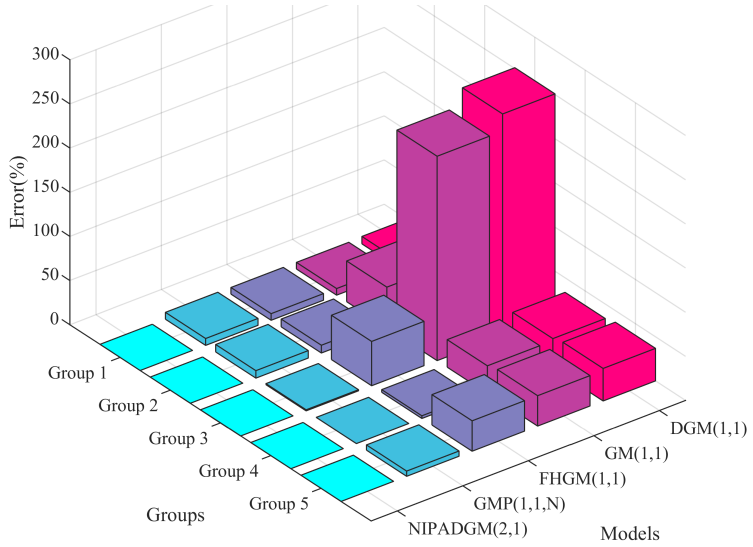

Figure 2. Errors for different models under different types of curves.

4. Case study

4.1. A ridge-regularized second-order discrete grey model with new information priority accumulation

Theorem 1 indicates that the design matrix B of the proposed model has dimension $(n-2)\times 5$. Compared with conventional first-order grey models, the second-order model yields a matrix B with fewer rows for an identical sample size, implying more stringent sample size requirements. Specifically, when $n \leq 7$, the number of rows in B falls below five. Under such circumstances, employing Eq (2.5) to estimate the parameter vector θ would result in near-singularity of $(B^T B)$, yielding inaccurate parameter estimates and risking multicollinearity in B. Consequently, for small-sample scenarios with $n \leq 7$, this study introduces Ridge regression regularization to enhance parameter estimation stability and model generalization capability.

Ridge regression, proposed by Hoerl and Kennard in 1970, is a biased estimation method that alleviates multicollinearity in the design matrix through L2 regularization [43]. To address the ill-conditioning or singularity of the information matrix $(B^T B)$ induced by small samples in grey models, this approach introduces a penalty term $\lambda \|\beta\|_2^2$ into the ordinary least squares objective function, ensuring that the modified matrix $(B^T B + \lambda I)$ is strictly positive definite, thereby guaranteeing unique and numerically stable parameter estimates. The objective function is formulated in Eq (4.1), with the analytical solution given by Eq (4.2). This method enhances model stability at the expense of unbiasedness—that is, by

accepting a small bias to reduce prediction error and improve overall accuracy.

$$\hat{\boldsymbol{\theta}}_{\text{Ridge}} = \arg\min_{\boldsymbol{\theta}} \left\{ \|\boldsymbol{Y} - \boldsymbol{B}\boldsymbol{\theta}\|^2 + \lambda \|\boldsymbol{\theta}\|^2 \right\}. \tag{4.1}$$

$$\hat{\theta}_{Ridge} = (B^T B + \lambda I)^{-1} BY. \tag{4.2}$$

Taking the six data points from the case study in [34] as an example, the NIPADGM(2,1) model with least squares parameter estimation is designated as NIPADGM(2,1)-I, and that with Ridge regression regularization is designated as NIPADGM(2,1)-II. These six observations are employed to estimate both models, with results reported in Table 2.

Table 2. Improvement effect of Ridge regression on NIPADGM(2,1) model accuracy.

Serial number	1	2	3	4	5	6	*MAPE*	*RMSE*
Data	488.56	565.26	664.52	764.03	908.71	1098.89		
NIPADGM(2,1)-I	488.56	565.26	667.1059	769.1738	929.1788	1096.246		
	0.00%	0.00%	0.39%	0.67%	2.25%	0.24%	0.59%	9.58
NIPADGM(2,1)-II	488.56	565.26	664.2722	764.1753	908.6072	1098.878		
	0.00%	0.00%	0.04%	0.02%	0.01%	0.00%	0.01%	0.14

The results in Table 2 indicate that, compared with the NIPADGM(2,1)-I model, the Ridge-regularized variant achieves significantly reduced fitting errors across all time points. Specifically, the *MAPE* decreases from 0.59% to 0.01%, and the *RMSE* from 9.58 to 0.14, validating that the introduction of Ridge regression regularization effectively alleviates design matrix ill-conditioning and enhances parameter estimation stability and model generalization under small-sample conditions ($n \leq 7$).

4.2. Numerical experiment

From Corollaries 1 and 2, it is clear that there is convergence of the fitted sequences of the model in some special cases. As a result, the fitted data of the model can be theoretically characterized by an "S"-shaped distribution. Among the grey models, the Verhulst model and the Gompertz model are often employed to fit the "S" data. Therefore, this paper takes the FDGGM model as an example of a case study [44]. Meanwhile, the EGM [8], NDGM [18], and FGM [25] models from reference [44] are adopted as comparative models. Data from 2011 to 2018 were utilized as the training set for modeling, followed by data from 2019 to 2020 as the validation set. The data were simultaneously entered into NIPADGM(2,1)-I and NIPADGM(2,1)-II for estimation and forecasting.

Table 3. The prediction of Jiangsu total population by grey models.

Year	Data	EGM		NDGM		FGM		FDGGM		NIPADGM(2,1)-I		NIPADGM(2,1)-II	
		Values	*APE (%)*	Values	*APE (%)*	Values	*APE (%)*	Values	*APE (%)*	Values	*APE (%)*	Values	*APE (%)*
2011	8023	8023.00	0.000%	8023.00	0.000%	8023.00	0.000%	8023.00	0.000%	8023.00	0.000%	8023.00	0.000%
2012	8120	8144.47	0.301%	8116.86	0.039%	8094.60	0.313%	8117.29	0.033%	8120.00	0.000%	8120.00	0.000%
2013	8192	8198.46	0.079%	8200.20	0.100%	8208.84	0.206%	8200.78	0.107%	8196.20	0.051%	8192.94	0.011%
2014	8281	8252.82	0.340%	8269.75	0.136%	8283.64	0.032%	8272.15	0.107%	8268.20	0.155%	8268.07	0.156%
2015	8315	8307.53	0.090%	8327.81	0.154%	8337.96	0.276%	8331.26	0.196%	8327.34	0.148%	8330.93	0.192%
2016	8381	8362.61	0.219%	8376.26	0.057%	8379.77	0.015%	8378.91	0.025%	8379.16	0.022%	8380.63	0.004%
2017	8423	8418.05	0.059%	8416.70	0.075%	8413.14	0.117%	8416.46	0.078%	8419.00	0.048%	8418.44	0.054%
2018	8446	8473.86	0.330%	8450.45	0.053%	8440.42	0.066%	8445.53	0.006%	8449.62	0.043%	8445.97	0.000%
MAPEsim			0.203%		0.088%		0.146%		0.079%		0.067%		**0.060%**
RMSEsim			19.381		8.015		15.084		8.233		**7.236**		7.953
2019	8469	8530.04	0.721%	8478.63	0.114%	8463.10	0.070%	8467.70	0.015%	8468.51	0.006%	8464.91	0.048%
2020	8477	8586.59	1.293%	8502.14	0.297%	8482.19	0.061%	8484.43	0.088%	8477.00	0.000%	8477.00	0.000%
MAPEpre			1.007%		0.205%		0.128%		0.051%		**0.003%**		0.024%
MAPEtot			0.381%		0.114%		0.128%		0.073%		0.053%		**0.052%**
RMSEpre			88.701		19.036		5.556		5.334		**0.350**		2.892
RMSEtot			42.855		10.837		12.863		7.290		**6.056**		7.145

As shown in Table 3, good results were achieved for each model. Since models such as EGM, NDGM, and FGM primarily fitted exponentially growing data, their fitting performance was significantly weaker than that of the FDGGM model and NIPADGM(2,1) model when applied to convergent data. Although the FDGGM model achieved excellent results during the training phase, its fitting performance in the validation phase was significantly weaker than that of the NIPADGM(2,1)-I model. NIPADGM(2,1)-I and NIPADGM(2,1)-II achieve the minimum errors at most time points, with *MAPEtot* of 0.053% and 0.052%, respectively, both significantly outperforming all competing models. Meanwhile, the root mean square error (*RMSE*) of both the NIPADGM(2,1)-I and NIPADGM(2,1)-II models consistently outperforms that of all competing models across all stages, indicating that the proposed model maintains strong fitting capability even when confronted with anomalous data. Overall, the NIPADGM(2,1) model has the best fitting effect, which verifies that the NIPADGM(2,1) model exhibits the most outstanding fitting performance when facing convergent data. In addition, compared with NIPADGM(2,1)-I, the NIPADGM(2,1)-II model incorporates Ridge regression regularization for parameter estimation. However, the computational results reveal that Ridge regularization does not yield substantial improvements in forecasting accuracy; rather, NIPADGM(2,1)-II exhibits inferior performance to NIPADGM(2,1)-I across all three *RMSE*-based metrics. This suggests that the proposed Ridge-regularized approach fails to further enhance model stability and accuracy when the modeling sample is sufficiently large.

4.2.1. Performance comparison between algorithms

A reasonable hyperparameter α can effectively improve model accuracy. Due to differences in algorithms, models also exhibit significant variations in the determining hyperparameter. Therefore, selecting an algorithm with fast convergence speed and high accuracy is crucial for solving for model hyperparameters. With the population size of each algorithm set to 100 and every algorithm executed 100 times, the differential evolution algorithm (DE) [39], particle swarm optimization algorithm (PSO) [45], artificial bee colony algorithm (ABC) [46], genetic algorithm (GA) [47], and whale optimization algorithm (WOA) [48] are compared under different numbers of iterations. Subsequently, the average value of the 100 results from each experimental group is used as the evaluation metric for the algorithm. The calculation results are summarized in Table 4.

Table 4. Performance comparison of four intelligent algorithms.

Iteration number	5		20		30		50		100	
	MAPE	Rank	*MAPE*	Rank	*MAPE*	Rank	*MAPE*	Rank	*MAPE*	Rank
DE	0.057%	3	0.053%	1	0.053%	1	0.053%	1	0.053%	1
PSO	0.056%	1	0.056%	3	0.056%	3	0.055%	3	0.055%	3
ABC	0.057%	3	0.054%	2	0.054%	2	0.054%	2	0.053%	1
GA	0.062%	5	0.059%	5	0.059%	5	0.056%	4	0.055%	3
WOA	0.056%	1	0.056%	3	0.056%	3	0.056%	4	0.055%	3

As shown in Table 4, when the iteration count is set to 5, although the accuracy of the differential evolution algorithm is lower than that of the particle swarm optimization and whale optimization algorithms, the errors among the various algorithms are not significantly different. Subsequently, the errors of all algorithms gradually decreased as the number of iterations increased. Throughout this

process, the differential evolution algorithm consistently outperformed the other algorithms. In contrast, the other four algorithms demonstrated significantly weaker convergence speed and result accuracy when faced with a nonlinear optimization problem. Therefore, this paper selects the differential evolution algorithm to solve for the model hyperparameter to ensure the accuracy of the modeling results.

4.2.2. Monte Carlo experiment

To verify the stability of the model's output, we conduct a Monte Carlo experiment on the NIPADGM(1,1) model, which is optimized using the differential evolution algorithm. The model is optimized 2000 times, and a frequency distribution of the resulting optimal objective function values is plotted, as shown in Figure 3.

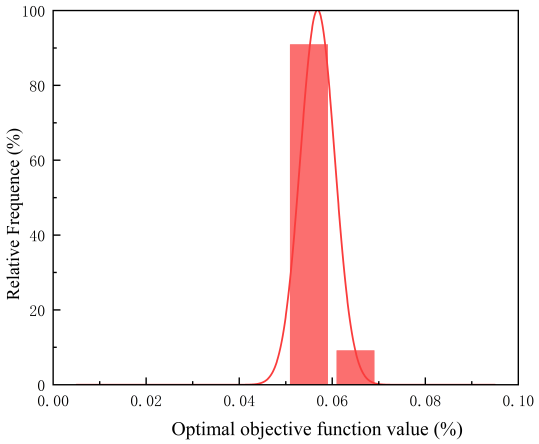

Figure 3. Frequency distribution of optimal objective function values.

In 2000 repeated optimization experiments, the optimal objective function value reached 0.0525% in 1818 trials, while 182 trials achieved an optimal value of 0.061%, with a fluctuation range of only 0.0085%. The most frequently occurring optimal objective function value aligns with the computational results of the NIPADGM(2,1) model in Table 3, indicating that the proposed model and the differential evolution algorithm exhibit good stability and repeatability.

5. Prediction and analysis of electricity generation in China

5.1. Data description

As a large country with abundant energy sources, China's accurate prediction of total electricity generation will contribute to the anticipation of the national power supply and demand situation and also to the rational allocation of power resources between the east and west. At the same time, by forecasting the amount of electricity generated from various energy sources, particularly renewable energy, we can better plan domestic energy production, reduce reliance on imported fossil fuels, and contribute to achieving the "dual carbon" goal. Today, China has made a series of achievements in renewable energy. According to the relevant documents issued by the National Development and Reform Commission of the People's Republic of China (`https://www.ndrc.gov.cn/fggz/hjyzy/jnhnx/`

202302/t20230215_1348799.html), in 2022, China's renewable energy installed capacity was 152 million kilowatts, accounting for 76.2% of the country's new power generation capacity. Nowadays, China's renewable energy generation capacity is increasing year by year within the energy generation structure. Consequently, accurate prediction of renewable energy generation can provide a scientific basis for the planning and construction of new energy projects and contribute to the realization of the "double carbon" goal. However, as an emerging industry, renewable energy still has some limitations in its development, such as energy storage and transportation. Given that natural gas is a relatively clean transitional energy source, predicting its electricity generation can assist policymakers in better planning the energy mix and gradually decreasing reliance on high-emission energy sources. In addition, coal, as a widely distributed and abundant natural resource, has always been the main source of energy generation in China. Compared with energy sources such as oil and natural gas, the supply of coal is relatively stable and the price volatility is small. Consequently, during the critical period of transitioning China's energy structure to decarbonization, the accurate prediction of coal power generation is essential to ensure the stability of the energy supply, considering that coal is a mature energy technology. This paper analyzes China's total electricity generation, electricity generation from renewable energy, electricity generation from natural gas, and electricity generation from coal from 2010 to 2024 in the Energy Institute Statistical Review of World Energy (https://www.energyinst.org/statistical-review), as shown in Table 5 and Figure 4.

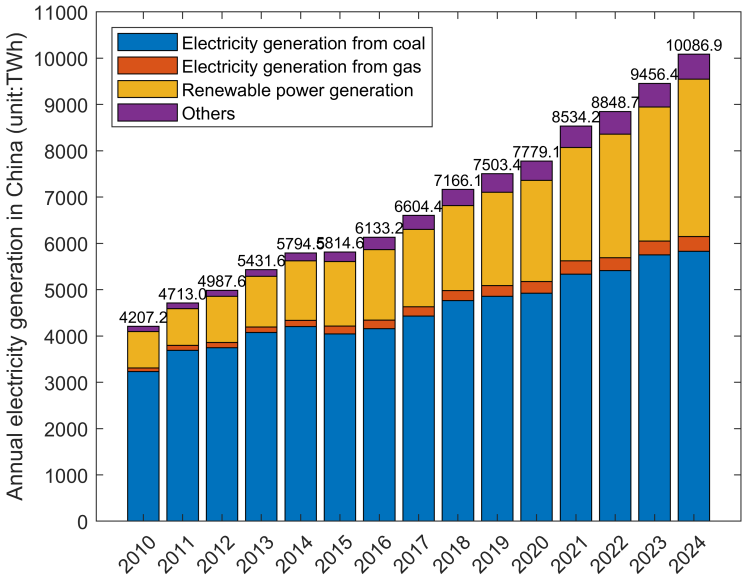

Figure 4. Growth in four types of electricity generation.

As shown in Figure 4, China's overall electricity generation has shown a steady growth trend, with an overall increase of 139.8% over the past 15 years. Coal, as a traditional energy source for electricity generation in China, has seen an overall increase in its electricity generation volume. However, the growth rate of electricity generation from coal is significantly lower than that of China's total power generation. Meanwhile, the electricity generation from renewable energy sources is increasing steadily at an annual rate of approximately 11%. Natural gas, which serves as a transitional energy source, has experienced a stable increase in its power generation volume overall. Nevertheless, the growth rate has

Table 5. China's total electricity generation and electricity generation from various energy sources (TWh).

	2010	2011	2012	2013	2014	2015	2016	2017	2018	2019	2020	2021	2022	2023	2024
Electricity generation	4207.2	4713	4987.6	5431.6	5794.5	5814.6	6133.2	6604.4	7166.1	7503.4	7779.1	8534.2	8848.7	9456.4	10,086.9
Electricity generation from coal	3233.6	3690.9	3748.2	4077.4	4203.1	4046.2	4156.4	4430	4763.9	4855.2	4922	5333.9	5412.7	5753.9	5827.6
Electricity generation from gas	77.7	108.8	110.3	116.4	133.3	166.9	188.3	203.2	215.5	232.5	252.5	287.1	275.6	297.8	320.7
Renewable power generation (incl hydro)	786.4	792.4	999.6	1093.4	1289.2	1393.7	1522.8	1667.1	1835.3	2014.6	2184.9	2448.7	2670.6	2894.1	3398.8

declined significantly in recent years. The aforementioned changes in energy generation also indirectly indicate that China is progressively shifting its energy structure toward a low-carbon transition.

5.2. Fitting and analysis of the model

The data on China's electricity generation during 2010–2021 are employed as the training set for modeling, while the data from 2022 to 2024 are employed as the validation set.

(1) The original data $X^{(0)} = (4207.20, 4713.00, \cdots, 10086.9)$ is brought into the flowchart of the NIPADGM(2,1) model. The differential evolution optimization algorithm is utilized to solve the optimal parameter $\alpha = 0.862$.

(2) The accumulated sequence $X^{(\alpha)}$ is first computed via Eq (2.1). Subsequently, given the adequate sample size, the parameter vector is estimated through Eq (2.5) using ordinary least squares.

$\theta = [\beta_1, \beta_2, \beta_3, \beta_4, \beta_5]^T = [\ 0.881, -0.098, 10.638, 502.636, 4315.102]^T$.

(3) Since the eigenequation in this case has two unequal real roots, the model parameter vector θ is brought into Eq (2.24) to calculate $\hat{X}^{(\alpha)}$.

$\hat{x}^{(0.862)}(k+1) = -9911.14 \cdot 0.75^k + 460.11 \cdot (0.13)^k + 48.99k^2 + 2005.86k + 13658.22$.

(4) The restored value $\hat{X}^{(0)}$ is calculated using Eq (2.2).

To better demonstrate the performance advantages of the new model, this study employs the following comparative models: recently developed grey models (IBCFGMP(1,1,N) [26], TVNDGM(1,1) [28], degenerate forms of the proposed model (GM(1,1) [8], DGM(1,1) [16], NDGM(1,1) [19], NIPDGM(1,1) [23], DNDGM(2,1) [34], and DGM(2,1) [41]), and time series models from other research domains (GBPNN [49], LR [50], and LSSVR [51]). The calculation data for each model are shown in Table 6 and Figure 5.

As depicted in Table 6, the NIPADGM(2,1) model exhibits the best fitting effect for the actual data. As illustrated in Figure 5, the electricity generation data exhibit a certain degree of nonlinearity. Consequently, the linear regression (LR) model fails to capture the nonlinear trend, yielding unsatisfactory predictions. When confronted with small samples, the LSSVR model is prone to ill-conditioning of the kernel matrix, rendering it sensitive to parameter selection and susceptible to overfitting training noise, thereby producing unstable validation performance. Therefore, the errors of both LR and LSSVR escalate progressively with increasing forecast horizons. The grey machine learning model (GBPNN) effectively enhances nonlinear data fitting capability through the integration of BP neural networks, while preserving the advantages of grey system theory for small-sample modeling. Consequently, the GBPNN model demonstrates superior accuracy compared to both the linear regression (LR) and least squares support vector regression (LSSVR) models; however, a performance gap remains relative to the proposed model in this study. The GM(1,1), DGM(1,1), NDGM(1,1), NGM(1,1), DGM(2,1), and NDGM(2,1) models can be regarded as special cases formed by constraining parameters of the NIPADGM(2,1)

Table 6. Electricity generation prediction in China (TWh).

Year	Data	NIPA-DGM(2,1)	IBCF-GMP(1,1,N)	TVN-DGM(1,1)	GM(1,1)	DGM(1,1)	NDGM(1,1)	NIP-DGM(1,1)	DGM(2,1)	DN-DGM(2,1)	GBPNN	LR	LSSVR
2010	4207.20	4207.20	4183.39	4207.20	4207.20	4207.20	4207.20	4207.20	4207.20	4207.20	4207.20	4218.10	——
2011	4713.00	4713.00	4702.15	4776.89	4727.00	4728.86	4776.83	4728.86	4713.00	4713.00	4727.00	4582.50	——
2012	4987.60	5110.82	5186.58	5033.09	5006.19	5008.15	5033.07	5008.15	5012.10	5081.40	5006.19	4946.90	——
2013	5431.60	5337.30	5431.67	5309.07	5301.88	5303.94	5309.07	5303.94	5307.80	5340.40	5286.01	5311.40	5465.20
2014	5794.50	5595.88	5640.07	5606.35	5615.02	5617.20	5606.37	5617.20	5620.60	5621.30	5840.92	5675.80	5686.70
2015	5814.60	5902.52	5890.85	5926.57	5946.67	5948.96	5926.60	5948.96	5951.90	5927.90	5955.39	6040.20	5940.40
2016	6133.20	6251.29	6207.10	6271.50	6297.90	6300.32	6271.54	6300.32	6302.60	6262.70	5863.22	6404.60	6178.80
2017	6604.40	6635.40	6587.65	6643.05	6669.87	6672.43	6643.09	6672.43	6674.10	6628.20	6583.11	6769.00	6644.00
2018	7166.10	7049.45	7022.29	7043.28	7063.82	7066.51	7043.30	7066.51	7067.40	7027.30	7120.66	7133.50	6968.70
2019	7503.40	7489.36	7498.75	7474.38	7481.03	7483.87	7474.38	7483.87	7484.00	7462.90	7682.22	7497.90	7507.30
2020	7779.10	7952.03	8005.71	7938.74	7922.88	7925.88	7938.72	7925.88	7925.00	7938.60	7732.60	7862.30	7962.60
2021	8534.20	8435.18	8533.81	8438.94	8390.83	8394.00	8438.88	8394.00	8392.10	8457.90	8250.56	8226.70	8407.30
MAPEsim		1.52%	**1.27%**	1.62%	1.58%	1.58%	1.62%	1.58%	1.56%	1.49%	1.66%	2.01%	1.40%
RMSEsim		112.68	**110.96**	112.90	117.02	116.98	112.90	116.98	116.84	108.48	145.76	158.52	115.94
2022	8848.70	8937.07	9075.78	8977.72	8886.42	8889.76	8977.63	8889.76	8886.70	9024.80	9150.49	8591.10	8638.10
2023	9456.40	9456.40	9626.23	9558.07	9411.29	9414.80	9557.94	9414.80	9410.40	9643.80	9361.58	8955.50	8641.40
2024	10086.90	9992.20	10,181.23	10,183.20	9967.15	9970.86	10,183.01	9970.86	9965.10	10,320.00	9581.75	9320.00	8797.40
MAPEpre		**0.65%**	1.77%	1.16%	0.70%	0.68%	1.16%	0.68%	0.71%	2.09%	3.14%	5.27%	7.93%
MAPEtot		**1.33%**	1.37%	1.52%	1.39%	1.39%	1.52%	1.39%	1.38%	1.62%	1.98%	2.66%	3.04%
RMSEpre		**74.78**	172.54	109.93	77.03	75.02	109.81	75.02	78.31	200.39	344.11	549.36	889.08
RMSEtot		**105.71**	125.71	112.27	109.68	109.35	112.24	109.35	109.73	133.61	205.11	283.66	455.74

model. Owing to structural limitations, these models exhibit inferior fitting performance compared to the NIPADGM(2,1) model. As can be clearly observed from Figure 5, although the IBCFGMP(1,1,N) model enhances data adaptability through the incorporation of quadratic polynomials, thereby achieving superior performance on the training set, its fitting efficacy on the validation set is markedly inferior to that of the NIPADGM(2,1) model. From Table 6, it can be seen that the mean absolute percentage errors of the total set of each model are 1.33%, 1.37%, 1.52%, 1.39%, 1.52%, 1.39%, 1.38%, 1.62%, 1.98%, 2.66%, and 3.04% respectively, which indicates that the NIPADGM(2,1) model has higher model accuracy than other models. Since the root mean square error is more sensitive to outliers, the NIPADGM(2,1) model achieves the best results under the *RMSEtot* metric, which demonstrates that the model is robust and less affected by outliers. Meanwhile, in the validation phase, the NIPADGM(2,1) model demonstrates excellent multi-step forecasting performance: the prediction error is 1.00% for the first step, decreases to 0% for the second step, and remains at 0.94% for the third step. Notably, the model's prediction errors do not exhibit an accumulating trend with increasing forecast horizons, indicating that the model possesses effective simultaneous multi-step forecasting capability and can achieve stable long-term predictions without relying on single-step recursion.

5.3. Robustness tests of the NIPADGM(2,1) model

To further validate the robustness of the proposed model for electricity generation forecasting, this section employs 70%, 80%, and 90% of the China electricity generation data as training sets for model estimation, and calculates the mean absolute percentage error at each stage under different training set proportions. The computational results are presented in Table 7.

As shown in Table 7, the NIPADGM(2,1) model exhibits remarkable stability in fitting accuracy across different sample sizes, with training set errors consistently around 1.5% under all three scenarios. This consistency indicates that the model's in-sample fitting capability is insensitive to sample size when sufficient data are available. When the training set proportion is 70% (i.e., using data from 2010–2020 for model estimation), the validation set error is relatively large, potentially attributable to the significant surge in China's electricity generation in 2021 (9.7% increase), which substantially exceeds growth rates in other years. Thus, the 2021 data point can be regarded as an anomalous observation. As

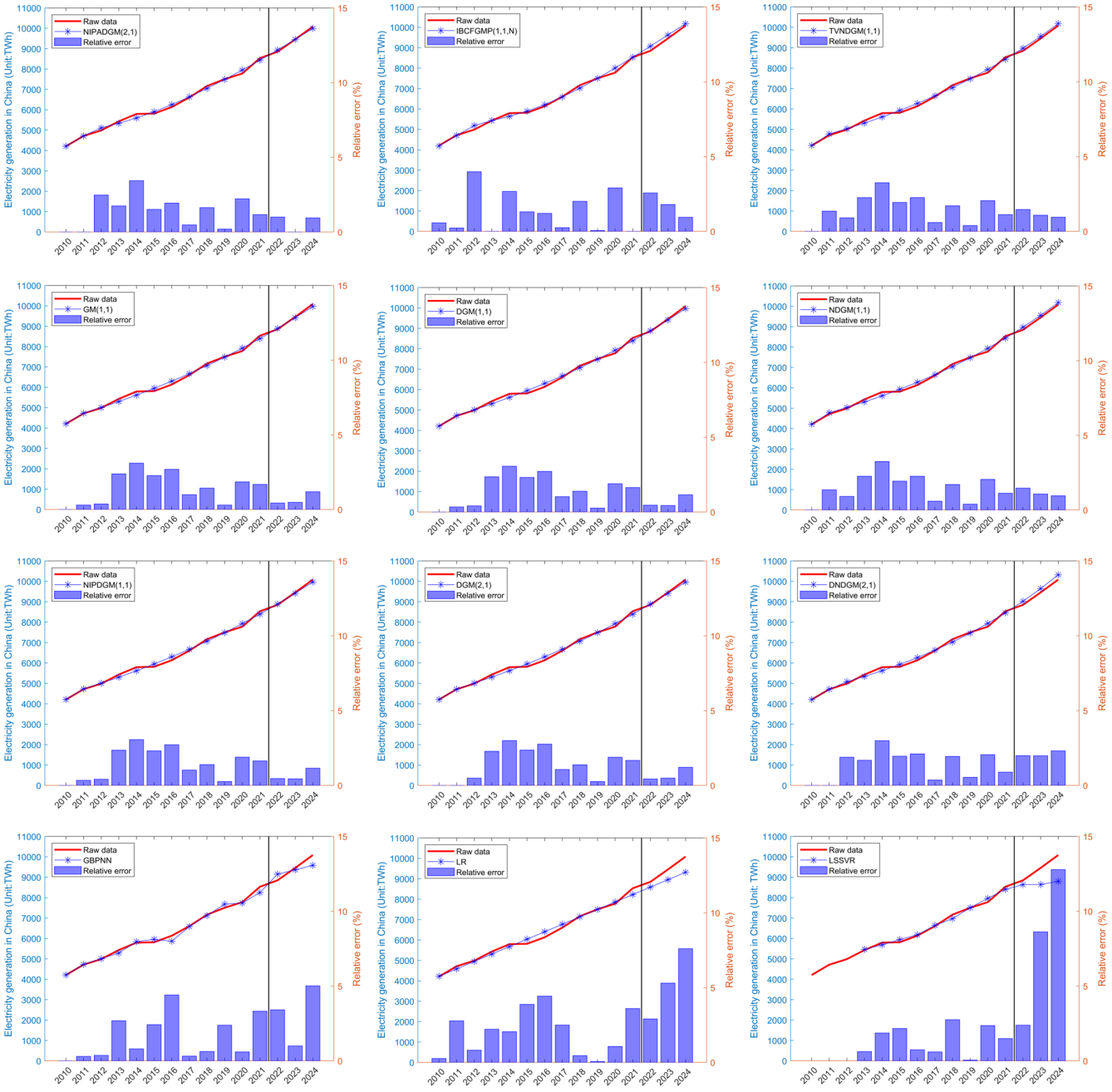

Figure 5. Fitting curves for different models of electricity generation.

this data point is excluded from the modeling dataset, a certain degree of deviation arises between the fitted and actual values. When the training set proportion is 80% or 90%, the modeling sample encompasses this anomalous data point, yielding fitted results that more closely approximate actual conditions, with comparable performance across the training, validation, and overall sets. Therefore, this study concludes that the proposed model exhibits favorable robustness and adaptability across varying training set proportions, provided that modeling samples are sufficient and development trends remain relatively smooth.

Table 7. Modeling results of the NIPADGM(2,1) model under different training set proportions.

Training set proportion	*MAPEsim*	*MAPEpre*	*MAPEtot*
70%	1.51%	3.60%	2.14%
80%	1.51%	0.65%	1.32%
90%	1.45%	0.23%	1.27%

5.4. Application of the NIPADGM(2,1) model to other energy generation

Given the satisfactory robustness and generalization capability exhibited by the NIPADGM(2,1) model, this research further investigates its applicability across diverse energy generation contexts. Coal, natural gas, and renewable electricity generation data from 2010 to 2021 are utilized as the training set, whereas data from 2022 to 2024 are employed as the validation set. Detailed results and performance metrics are presented in Table 8.

Table 8. Fitting of the electricity generation of three energy sources (Unit: TWh).

Year	Data	NIPA-DGM(2,1)	IBCF-GMP(1,1,N)	TVN-DGM(1,1)	GM(1,1)	DGM(1,1)	NDGM(1,1)	NIP-DGM(1,1)	DGM(2,1)	DN-DGM(2,1)	GBPNN	LR	LSSVR
Electricity generation from coal													
2010	3233.60	3233.60	3187.62	3233.60	3233.60	3233.60	3233.60	3233.60	3233.60	3233.60	3233.60	3400.79	——
2011	3690.90	3690.90	3690.90	3723.60	3654.15	3655.34	3722.63	3655.34	3690.90	3690.90	3654.15	3562.18	——
2012	3748.20	3878.98	3902.48	3819.29	3784.86	3785.96	3818.91	3785.96	3775.27	3838.33	3784.86	3723.56	——
2013	4077.40	3946.15	4009.64	3924.86	3920.25	3921.25	3924.91	3921.25	3905.38	3939.92	4027.82	3884.94	4052.60
2014	4203.10	4030.52	4091.34	4041.26	4060.48	4061.38	4041.61	4061.38	4047.67	4049.26	4032.05	4046.33	4210.50
2015	4046.20	4146.06	4181.92	4169.58	4205.72	4206.51	4170.09	4206.51	4196.48	4171.27	4101.44	4207.71	4153.10
2016	4156.40	4289.02	4296.55	4311.01	4356.17	4356.83	4311.54	4356.83	4350.99	4307.74	4491.34	4369.09	4163.50
2017	4430.00	4454.42	4441.14	4466.82	4511.99	4512.52	4467.27	4512.52	4511.23	4460.38	4429.40	4530.47	4471.40
2018	4763.90	4638.25	4616.90	4638.47	4673.39	4673.78	4638.72	4673.78	4677.38	4631.13	4782.49	4691.86	4589.30
2019	4855.20	4837.55	4822.74	4827.50	4840.56	4840.80	4827.48	4840.80	4849.66	4822.13	4855.02	4853.24	4868.90
2020	4922.00	5050.14	5056.43	5035.65	5013.71	5013.79	5035.29	5013.79	5028.27	5035.77	4877.13	5014.62	4992.80
2021	5333.90	5274.45	5315.34	5264.81	5193.06	5192.95	5264.08	5192.95	5213.47	5274.76	5310.07	5176.01	5286.00
2022	5412.70	5509.32	5596.81	5517.07	5378.82	5378.53	5515.96	5378.53	5405.48	5542.08	5439.15	5337.39	5384.00
2023	5753.90	5753.90	5898.29	5794.70	5571.22	5570.73	5793.27	5570.73	5604.57	5841.11	5404.20	5498.77	5172.60
2024	5827.60	6007.58	6217.46	6100.23	5770.51	5769.80	6098.57	5769.80	5810.99	6175.61	5880.26	5660.16	5353.70
MAPE		**2.04**%	2.12%	2.29%	2.24%	2.24%	2.29%	2.24%	2.17%	2.40%	1.85%	2.95%	2.47%
RMSE		**110.21**	112.50	124.5401	117.7898	117.8746	124.1921	117.8746	116.8407	144.3227	141.0008	147.3472	226.41
Electricity generation from gas													
2010	77.70	77.70	77.65	77.70	77.70	77.70	77.70	77.70	77.70	77.70	77.70	74.78	——
2011	108.80	108.80	108.80	98.50	105.93	106.11	98.53	88.74	108.80	108.80	105.93	92.89	——
2012	110.30	111.67	109.89	112.90	117.07	117.27	112.91	107.89	118.38	107.91	117.07	111.00	——
2013	116.40	113.55	121.43	128.05	129.37	129.59	128.05	126.96	129.87	121.50	115.63	129.11	120.40
2014	133.30	134.70	139.43	144.00	142.97	143.21	144.00	145.97	143.06	139.67	129.25	147.21	139.70
2015	166.90	166.42	160.14	160.79	158.00	158.26	160.78	164.91	157.91	159.29	141.99	165.32	156.40
2016	188.30	189.86	181.42	178.47	174.61	174.89	178.46	183.78	174.48	179.37	178.77	183.43	187.80
2017	203.20	201.71	202.19	197.08	192.97	193.27	197.07	202.58	192.88	199.60	203.99	201.54	202.60
2018	215.50	213.78	221.87	216.67	213.26	213.58	216.67	221.32	213.28	219.89	176.12	219.64	217.80
2019	232.50	234.43	240.12	237.30	235.67	236.03	237.30	239.99	235.87	240.21	199.38	237.75	234.10
2020	252.50	259.38	256.73	259.02	260.45	260.83	259.03	258.60	260.87	260.54	238.56	255.86	255.50
2021	287.10	280.53	271.49	281.89	287.83	288.25	281.90	277.14	288.52	280.88	274.34	273.96	281.50
2022	275.60	296.85	284.23	305.98	318.09	318.54	305.98	295.61	319.11	301.23	301.44	292.07	313.70
2023	297.80	313.59	294.77	331.34	351.53	352.01	331.34	314.02	352.95	321.60	334.00	310.18	324.00
2024	320.70	334.16	302.94	358.04	388.48	389.01	358.04	332.36	390.38	341.98	373.03	328.29	309.90
MAPE		**2.41**%	2.74%	6.27%	8.23%	8.29%	6.27%	5.11%	8.34%	4.33%	8.39%	4.47%	4.20%
RMSE		8.43	**7.82**	17.05	26.79	27.01	17.05	11.12	27.51	12.19	24.65	9.51	137.93
Renewable power generation (incl hydro)													
2010	786.40	786.40	786.47	786.40	786.40	786.40	786.40	786.40	786.40	786.40	786.40	677.44	——

Continued on next page

Table 8 – continued from the previous page

Year	Data	NIPA-DGM(2,1)	IBCF-GMP(1,1,N)	TVN-DGM(1,1)	GM(1,1)	DGM(1,1)	NDGM(1,1)	NIP-DGM(1,1)	DGM(2,1)	DN-DGM(2,1)	GBPNN	LR	LSSVR
2011	792.40	792.40	794.74	879.98	909.53	910.63	842.39	855.50	792.40	792.40	909.53	827.42	——
2012	999.60	999.25	981.36	993.52	1004.65	1005.90	966.87	970.38	1005.67	1007.66	1004.65	977.40	——
2013	1093.40	1107.46	1131.55	1113.22	1109.71	1111.14	1097.54	1093.40	1134.39	1123.67	1093.40	1127.38	1127.60
2014	1289.20	1270.12	1264.57	1240.20	1225.77	1227.38	1234.70	1225.12	1253.31	1246.24	1289.20	1277.37	1261.70
2015	1393.70	1387.28	1392.91	1375.62	1353.96	1355.80	1378.67	1366.16	1379.22	1378.45	1393.70	1427.35	1380.80
2016	1522.80	1536.11	1525.49	1520.67	1495.55	1497.64	1529.79	1517.17	1516.62	1521.12	1526.74	1577.33	1537.10
2017	1667.10	1670.97	1668.97	1676.63	1651.96	1654.33	1688.42	1678.87	1667.45	1675.06	1668.67	1727.32	1673.30
2018	1835.30	1832.63	1828.41	1844.81	1824.72	1827.41	1854.93	1852.02	1833.23	1841.18	1835.30	1877.30	1823.20
2019	2014.60	2002.41	2007.65	2026.60	2015.55	2018.59	2029.70	2037.41	2015.49	2020.44	2014.60	2027.28	2008.20
2020	2184.90	2204.03	2209.51	2223.52	2226.34	2229.78	2213.16	2235.91	2215.86	2213.87	2184.90	2177.26	2220.10
2021	2448.70	2432.63	2435.98	2437.16	2459.17	2463.06	2405.73	2448.46	2436.15	2422.59	2448.70	2327.25	2417.60
2022	2670.60	2704.38	2688.32	2669.23	2716.35	2720.75	2607.87	2676.05	2678.34	2647.83	2661.72	2477.23	2552.80
2023	2894.10	3021.97	2967.09	2921.59	3000.43	3005.40	2820.05	2919.74	2944.61	2890.87	3076.26	2627.21	2556.60
2024	3398.80	3398.80	3272.30	3196.25	3314.21	3319.83	3042.76	3180.66	3237.35	3153.13	3349.44	2777.20	2484.30
MAPE		**0.88**%	1.14%	2.11%	2.72%	2.74%	2.66%	2.20%	1.25%	1.41%	1.69%	4.52%	4.53%
RMSE		**36.90**	40.76	62.43	55.47	55.95	102.38	66.30	48.59	68.45	59.44	193.19	263.06

The model has achieved the outstanding results in multiple indicators across three cases. Therefore, this paper utilizes the model to generate six-year forecasts for four power generation cases, with the results detailed in Table 9.

Table 9. Forecast total electricity generation and energy generation in China (Unit: TWh).

Year	2025	2026	2027	2028	2029	2030
Electricity generation	10,543.73	11,110.46	11,691.96	12,287.93	12,898.14	13,522.42
Electricity generation from coal	6269.92	6540.59	6819.34	7106.02	7400.49	7702.66
Electricity generation from gas	356.52	377.19	395.89	414.95	435.77	457.36
Renewable power generation (incl hydro)	3842.24	4365.42	4979.16	5697.77	6535.17	7507.77

The forecast results show that in the next six years, China's total electricity generation will reach 13,522.42 TWh in 2030, with an overall increase of 34%. At the same time, the electricity generation of coal, natural gas, and renewable energy will reach 7702.66 TWh, 457.36 TWh and 7507.77 TWh respectively, with an increase of 32.2%, 42.6%, and 120.9%, respectively. The growth rate of electricity generation from coal is significantly lower than that of renewable energy generation. Over the next six years, the proportion of renewable energy in total electricity generation will continue to grow at an average annual rate of 4%, reaching 55.5% by 2030.

6. Conclusions and prospects

To effectively capture the nonlinear and complex patterns inherent in small-sample data, this paper proposes a new information priority accumulation discrete grey model with self-adaptive capabilities. The model parameters have been estimated using the least squares method, and the time-response sequences of the model under various conditions have been derived. Through the analysis of several cases, this paper presents the following conclusions.

1) The models are highly adaptable. Many grey models are special cases of the NIPADGM(2,1) model. At the same time, the model can fit different types of curves in different situations.

2) As shown in Property 2, the model has the ability to fit the "S" curve when both real roots of the characteristic equation of the model lie in the range from -1 to 1, which broadens the variety of grey models that can be applied to the "S" curves.

3) This study rigorously establishes that the proposed model is unbiased with respect to five specific curve types. Perfect fitting is achievable when data strictly conform to these distributions, while high-precision fitting is likewise attainable when data approximate these patterns.

4) Under small-sample modeling conditions ($n \leq 7$), the introduction of Ridge regression regularization effectively alleviates design matrix ill-conditioning, thereby enhancing parameter estimation stability and model generalization for NIPADGM(2,1). However, when modeling samples are sufficient, the improvement afforded by Ridge regularization becomes marginal.

5) Through performance comparisons among algorithms and Monte Carlo experiments, the NIPADGM(2,1) model based on the differential evolution algorithm has been validated to exhibit outstanding accuracy and stability.

In this paper, although the model has strong adaptive ability and high fitting accuracy, the model still possesses the following limitations. First of all, the model is a univariate model. In the process of modeling, this paper excludes the influence of other factors on the target factor, so future work will also be devoted to the study of the grey higher-order multivariate model. Subsequently, real data are often accompanied by time delay effects, which are not taken into account in this paper. Therefore, in the future, in view of the above shortcomings, the authors will focus on improving the above deficiencies and strive to realize the combination of grey models with machine learning field models, in order to further expand the application scope of grey system theory.

Use of AI tools declaration

The authors declare they have not used Artificial Intelligence (AI) tools in the creation of this article.

Acknowledgments

This work was supported by the Key Scientific Research Projects of Colleges and Universities in Henan Province (Grant No. 24A110004), and the Scientific and Technological Project in Henan Province of China (Grant No. 252102111064.).

Conflict of interest

The authors declare there is no conflict of interest.

References

1. J. W. Zeng, Z. Y. Chen, Y. J. Wang, R. Wang, Capacity, spatial patterns and benefits assessment of photovoltaic power under carbon neutrality goal in China, *Sci. Technol. Rev.*, **42** (2024), 34–46. https://doi.org/10.3981/j.issn.1000-7857.2024.02.00233
2. Z. Y. Zhuo, N. Zhang, X. R. Xie, H. H. Li, C. Q. Kang, Key technologies and developing challenges of power system with high proportion of renewable energy, *Autom. Electr. Power Syst.*, **45** (2021), 171–191. https://doi.org/10.7500/AEPS20200922001
3. G. Dudek, Pattern-based local linear regression models for short-term load forecasting, *Electr. Power Syst. Res.*, **130** (2016), 139–147. https://doi.org/10.1016/j.epsr.2015.09.001

4. C. Y. Wang, Q. Q. Duan, K. Zhou, J. Yao, M. Su, Y. C. Fu, et al., A hybrid model for photovoltaic power prediction of bothconvolutional and long short-term memory neural networksoptimized by genetic algorithm, *Acta Phys. Sin.*, **69** (2020), 149–155. https://doi.org/10.7498/aps.69.20191935
5. X. Luo, Z. J. Hu, Z. J. Ma, Z. Lv, Photovoltaic cluster power generation prediction based on hybrid deep learning, *J. Southwest Univ. (Nat. Sci. Ed.)*, **47** (2025), 200–210. https://doi.org/10.13718/j.cnki.xdzk.2025.03.018
6. A. Saxena, A nonlinear hyperbolic optimized grey model for market clearing price prediction: Analysis and case study, *Sustainable Energy Grids Networks*, **38** (2024), 101367. https://doi.org/10.1016/j.segan.2024.101367
7. L. Q. Huang, Q. Liao, H. R. Zhang, M. K. Jiang, J. Yan, Y. T. Liang, Forecasting power consumption with an activation function combined grey model: A case study of China, *Int. J. Electr. Power Energy Syst.*, **130** (2021), 106977. https://doi.org/10.1016/J.IJEPES.2021.106977
8. J. L. Deng, Control problems of grey systems, *Syst. Control Lett.*, **1** (1982), 288–294. https://doi.org/10.1016/s0167-6911(82)80025-x
9. D. Luo, X. Q. Qiao, Time-Delay TLDBGM (1, N) model with dynamic background value and its application, *J. Grey Syst.*, **36** (2024), 63–78.
10. M. L. Qiu, D. W. Li, Z. L. Luo, X. J. Yu. Huizhou GDP forecast based on fractional opposite-direction accumulating nonlinear grey bernoulli markov model, *Electron. Res. Arch.*, **31** (2023), 947–960. https://doi.org/10.3934/era.2023047
11. Q. F. Xu, Y. J. Guan, Y. B. Xu, R. Wang, A new grey forecasting model with fractional order accumulation generation operation and its application in GDP forecasting, *J. Grey Syst.*, **36** (2024), 70–79.
12. C. Li, Q. Qi, A novel hybrid grey system forecasting model based on seasonal fluctuation characteristics for electricity consumption in primary industry, *Energy*, **287** (2024), 129585. https://doi.org/10.1016/j.energy.2023.129585
13. L. Xia, Y. Y. Ren, Y. H. Wang, Forecasting China's total renewable energy capacity using a novel dynamic fractional order discrete grey model, *Expert Syst. Appl.*, **239** (2024), 122019. https://doi.org/10.1016/j.eswa.2023.122019
14. W. Ba, B. J. Chen, Q. Li, Comprehensive evaluation method for traffic flow data quality based on grey correlation analysis and particle swarm optimization, *J. Syst. Sci. Syst. Eng.*, **33** (2024), 106–128. https://doi.org/10.1007/s11518-023-5585-5
15. Q. Q. Shen, Y. G. Dang, Y. Cao, R. Q. Zhu, Improved grey Verhulst model based on new information priority fractional order accumulation, *Syst. Eng. Theory Pract.*, **45** (2025), 539–553. https://doi.org/10.12011/SETP2023-2039
16. N. M. Xie, S. F. Liu, Discrete grey forecasting model and its optimization, *Appl. Math. Modell.*, **33** (2008), 1173–1186. https://doi.org/10.1016/j.apm.2008.01.011
17. S. L. Li, S. Y. Yang, B. Zeng, W. Meng, Y. Bai, Unbiased and adaptive of discrete grey prediction model and its application, *Chin. J. Manage. Sci.*, **32** (2024), 149–160. https://doi.org/10.16381/j.cnki.issn1003-207x.2022.1937

18. X. B. Yang, A note on discrete grey prediction model of inhomogeneous exponents and its application, *Math. Pract. Theory*, **54** (2024), 148–160. https://doi.org/10.20266/j.math.2024.11.011

19. D. Luo, B. L. Wei, A unified treatment approach for a class of discrete grey forecasting models and its application, *Syst. Eng. Theory Pract.*, **39** (2019), 451–462. https://doi.org/10.12011/1000-6788-2017-1065-12

20. Z. D. Xu, Y. G. Dang, D. L. Yang, Discrete grey forecasting model with fractional order polynomial and its application, *Control Decis.*, **38** (2023), 3578–3584. https://doi.org/10.13195/j.kzyjc.2022.0080

21. Y. P. Ding, Y. G. Dang, J. J. Wang. Adaptive multivariable grey prediction model driven by Euler polynomials and its application, *Chin. J. Manage. Sci.*, **33** (2025), 185–199. https://doi.org/10.16381/j.cnki.issn1003-207x.2023.1297

22. L. Xia, Y. Y. Ren, Y. H. Wang, Y. Y. Fu, K. Zhou. A novel dynamic structural adaptive multivariable grey model and its application in China's solar energy generation forecasting, *Energy*, **312** (2024), 133534. https://doi.org/10.1016/j.energy.2024.133534

23. W. J. Zhou, H. R. Zhang, Y. G. Dang, Z. X. Wang, New information priority accumulated grey discrete model and its application, *Chin. J. Manage. Sci.*, **25** (2017), 140–148. https://doi.org/10.16381/j.cnki.issn1003-207x.2017.08.015

24. L. Xi, S. Ding, N. Xu, P. P. Xiong, Research on optimization of non-equidistant GM(1, 1) model based on the principle of new information priority, *Control Decis.*, **34** (2019), 2221–2228. https://doi.org/10.13195/j.kzyjc.2018.0163

25. L. F. Wu, S. F. Liu, L. G. Yao, S. L. Yan, D. L. Liu, Grey system model with the fractional order accumulation, *Commun. Nonlinear Sci. Numer. Simul.*, **18** (2013), 1775–1785. https://doi.org/10.1016/j.cnsns.2012.11.017

26. X. Ma, W. Q. Wu, B. Zeng, Y. Wang, X. X. Wu, The conformable fractional grey system model, *ISA Trans.*, **96** (2020), 255–271. https://doi.org/10.1016/j.isatra.2019.07.009

27. C. Yan, L. F. Wu, L. Y. Liu, K. Zhang, Fractional Hausdorff grey model and its properties, *Chaos, Solitons Fractals*, **138** (2020) 109915. https://doi.org/10.1016/j.chaos.2020.109915

28. L. Xia, Y. H. Wang, Y. X. Han, K. Zhou, Y. Y. Ren, Y. Y. Fu, A novel time-varying non-homogeneous discrete grey model and its application in forecasting solar energy generation in total north America, *J. Grey Syst.*, **37** (2025), 96–107.

29. Y. Z. Chen, W. H. Gong, S. Z. Li, S. B. Guo, A novel conformable fractional-order accumulation grey model and its applications in forecasting energy consumption of China, *Sci. Rep.*, **14** (2024), 31028. https://doi.org/10.1038/S41598-024-82128-W

30. L. Zeng, A gray model for increasing sequences with nonhomogeneous index trends based on fractional-order accumulation, *Math. Methods Appl. Sci.*, **41** (2018), 3750–3763. https://doi.org/10.1002/mma.4862

31. D. W. Li, M. L. Qiu, J. M. Jiang, S. P. Yang, The application of an optimized fractional order accumulated grey model with variable parameters in the total energy consumption of Jiangsu Province and the consumption level of Chinese residents, *Electron. Res. Arch.*, **30** (2022), 798–812. https://doi.org/10.3934/era.2022042

32. S. Z. Li, S. B. Guo, Y. Z. Chen, Optimization and application of Hausdorff fractional grey prediction model, *J. Henan Inst. Sci. Technol. (Nat. Sci. Ed.)*, **51** (2023), 76–84.

33. Y. Z. Chen, S. Z. Li, S. B. Guo, A novel fractional hausdorff discrete grey model for forecasting the renewable energy consumption, *J. Math.*, **2022** (2022), 8443619. https://doi.org/10.1155/2022/8443619

34. T. Su, Y. Wei, Direct discrete model of second order non-homogeneous sequence and application of grey prediction, *Syst. Eng. Theory Pract.*, **40** (2020), 2450–2465. https://doi.org/10.12011/1000-6788-2019-2319-16

35. L. Zeng, S. G. Luo, A discrete GM(2,1) model with fractional-order accumulation and its application, *J. Chongqing Normal Univ. (Nat. Sci.)*, **38** (2021), 73–80+2. https://doi.org/10.11721/cqnuj20210502

36. M. L. Cheng, Grey GM(2, 1) model with complex solution and its applications, *Chin. J. Eng. Math.*, **40** (2023), 763–778. https://doi.org/10.3969/j.issn.1005-3085.2023.05.006

37. N. Xu, Y. G. Dang, An optimized grey GM (2, 1) model and forecasting of highway subgrade settlement, *Math. Probl. Eng.*, **2015** (2015), 606707. https://doi.org/10.1155/2015/606707

38. L. W. Tang, Y. Y. Lu, The optimization of GM(2,1) model based on parameter estimation of grade difference format, *Syst. Eng. Theory Pract.*, **38** (2018), 502–508. https://doi.org/10.12011/1000-6788(2018)02-0502-07

39. L. Zeng, C. Liu, W. Z. Wu. A novel discrete GM (2, 1) model with a polynomial term for forecasting electricity consumption, *Electr. Power Syst. Res.* **214** (2023), 108926. https://doi.org/10.1016/j.epsr.2022.108926

40. S. J. Li, Y. Z. Miao, G. Y. Li, M. Ikram, A novel varistructure grey forecasting model with speed adaptation and its application, *Math. Comput. Simul.*, **172** (2020), 45–70. https://doi.org/10.1016/j.matcom.2019.12.020

41. H. B. Zhou, G. R. Xiao, X. X. Lin, Y. H. Yin, Landslide hazard assessment method based on feature screening and differential evolution algorithm optimization, *J. Geo-inf. Sci.*, **24** (2022), 2373–2388. https://doi.org/10.12082/dqxxkx.2022.220158

42. Y. F. Huang, C. N. Wang, H. S. Dang, S. T. Lai, Evaluating performance of the DGM (2, 1) model and its modified models, *Appl. Sci.*, **6** (2016), 73. https://doi.org/10.3390/app6030073

43. P. P. Xiong, Y. R. Wu, C. W. Tan, W. J. Tong, K. Y. Yang, A novel discrete mulivariate grey forecasting model with L_2 regularization term, *J. Syst. Sci. Math. Sci.*, **44** (2024), 1130–1146. https://doi.org/10.12341/jssms22406

44. W. L. Zhang, S. F. Liu, L. Y. Liu, R. M. K. T. Rathnayaka, N. M. Xie, J. L. Du, A novel fractional-order discrete grey Gompertz model for analyzing the aging population in Jiangsu Province, China, *Grey Syst. Theory Appl.*, **13** (2023), 544–557. https://doi.org/10.1108/GS-01-2023-0005

45. A. R. Jordehi, Enhanced leader PSO (ELPSO): A new PSO variant for solving global optimisation 660 problems, *Appl. Soft Comput.*, **26** (2015), 401–417. https://doi.org/10.1016/j.asoc.2014.10.026

46. K. Dervis, G. Beyza, O. Celal, N. K. Karaboga, B. Gorkemli, C. Ozturk, et al., A comprehensive survey: artificial bee colony (ABC) algorithm and applications, *Artif. Intell. Rev.*, **42** (2014), 21–57. https://doi.org/10.1007/s10462-012-9328-0

47. H. AL-Tabtabai, A. Alex, Using genetic algorithms to solve optimization problems in construction, *Eng. Constr. Archit. Manage.*, **6** (1999), 121–132. https://doi.org/10.1046/j.1365-232x.1999.00086.x

48. S. Mirjalili, A. Lewis, The whale optimization algorithm, *Adv. Eng. Software*, **95** (2016), 51–67. https://doi.org/10.1016/j.advengsoft.2016.01.008

49. S. Tian, C. W. Li, W. Huang, L. Wang, Forecasting method of highway freight volume based on GC-rBPNN model during COVID-19 epidemic, *J. Guangxi Normal Univ. (Nat. Sci. Ed.)*, **39** (2021), 24–32. https://doi.org/10.16088/j.issn.1001-6600.2020102902

50. I. Ilic, B. Görgülü, M. Cevik, M. G. Baydoğan, Explainable boosted linear regression for time series forecasting, *Pattern Recognit.*, **120** (2021), 108144. https://doi.org/10.1016/j.patcog.2021.108144

51. J. A. K. Suykens, J. Vandewalle, Least squares support vector machine classifiers, *Neural Process. Lett.*, **9** (1999), 293–300. https://doi.org/10.1023/A:1018628609742

AIMS Press